Earth-Science Reviews 126 (2013) 275–299

Contents lists available at ScienceDirect

Earth-Science Reviews

journal homepage: www.elsevier.com/locate/earscirev

Late Cretaceous climate changes recorded in Eastern Asian lacustrine deposits and North American Epieric sea strata

Chengshan Wang [a,f,*], Robert W. Scott [b,g,**], Xiaoqiao Wan [a,f], Stephan A. Graham [c], Yongjian Huang [a,f], Pujun Wang [d], Huaichun Wu [a,f], Walter E. Dean [e], Laiming Zhang [a,f]

[a] State Key Laboratory of Biogeology and Environmental Geology, China University of Geosciences, Beijing 100083, China
[b] Department of Geosciences, University of Tulsa, Tulsa, OK 74104, USA
[c] Department of Geological and Envrironmental Sciences, Stanford University, 397 Panama Mall, CA 94305, USA
[d] College of Earth Sciences, Jilin University, Changchun 130061,China
[e] U.S. Geological Survey, P.O. Box 25046, MS 980, Denver, CO 80225-0046, USA
[f] School of the Earth Science and Resources, China University of Geosciences, Beijing 100083, China
[g] Precision Stratigraphy Associates, Tulsa, OK 74104, USA

ARTICLE INFO

Article history:
Received 17 July 2013
Accepted 31 August 2013
Available online 13 September 2013

Keywords:
Late Cretaceous
Paleoclimate
Western Interior Seaway
Songliao Basin
Correlation of terrestrial and marine deposits
Greenhouse world

ABSTRACT

Cretaceous climate data of the long-lived Cretaceous Songliao Basin (SB) in eastern Asia is correlated and compared with the Western Interior Seaway (WIS) on the northern American plate, in order to understand better the dynamics of the Earth's past 'greenhouse' climates. Nearly continuous Late Cretaceous terrestrial deposition in the Songliao Basin is represented by two cores totaling 2431 m in length. The Turonian–Maastrichtian age of the section is based on integrated stratigraphy, and is comparable in age with Upper Cretaceous strata in the WIS. Being consistent with global trends, the dynamic Late Cretaceous climates of both the SB and WIS gradually cooled from the warmest Albian–Cenomanian time to the end of the Maastrichtian with several intervening warm periods as did the global climate. However regional differences existed, the Songliao Basin climate was humid to semi-humid, warm temperate–subtropical and the Western Interior Seaway was in the humid, warm temperate zone and experienced only moderate climatic changes. The shifts of oxygen isotope data in the Songliao Basin were frequent and abrupt, whereas WIS records more gradual change affected mainly by fresh-water runoff mixing with southern Tethyan and northern Arctic waters. Sedimentary cycles of eccentricity, obliquity and precession bands are recorded in both the SB and WIS basins. The sedimentary cycles in the WIS and SB are interpreted to be related to variations of the wet/dry runoff cycles, which indicate that orbital forcing played an important role in global climate change in Late Cretaceous. The most favorable condition for organic carbon burial in both the SB and WIS basin was bottom water anoxia regardless of the cause of the anoxia. But the organic carbon burial rate was usually much higher in the Songliao Lake than in the WI epeiric sea suggesting that giant lakes may serve as important sinks of atmospheric CO_2. In both basins organic-rich deposits formed during a rise in water level and incursion of saline waters. The integration of paleoclimate data from Cretaceous marine deposits and terrestrial sedimentary record will promote our understanding of the Cretaceous 'greenhouse' climate change and may provide insights for a future greenhouse world.

Contents

* Corresponding author. Tel.: +86 10 8232 1612; fax: +86 10 8232 2171.
** Corresponding author. Tel.: +1 918 243 5418; fax: +1 918 631 2091.
E-mail addresses: chshwang@cugb.edu.cn (C. Wang), rwscott@cimtel.net (R.W. Scott).

0012-8252/$ – see front matter © 2013 Elsevier B.V. All rights reserved.
http://dx.doi.org/10.1016/j.earscirev.2013.08.016

1. Introduction

Throughout its long geological history, the Earth has had two fundamentally different climate states—a cool 'icehouse' state characterized by high latitude ice sheets and a 'greenhouse' state characterized by much warmer global temperatures and only small or no ice sheets. For most of the past 600 million years of geological time climate has fluctuated between a warmer greenhouse state and icehouse state (NRC, 2011). Intervals of warmer global temperatures are of great interest, as they may provide analogs for a future greenhouse world. Paleotemperature estimates (Huber et al., 1995; Barrera and Savin, 1999; Cramer et al., 2009; Friedrich et al., 2012) from a variety of geochemical proxies indicate that Cretaceous time was one of the classic "greenhouse states" of the Earth (Skelton et al., 2003). During this 80 myr interval atmospheric and oceanic temperatures varied over a wide range and carbon dioxide content changed drastically in both marine and atmospheric reservoirs. The N-S temperature gradient was lower than today and surface wind patterns and ocean circulation probably were quite different from the modern oceans (Hay, 2009; Trabucho Alexandre et al., 2010; Flögel et al., 2011a,b; Wagner et al., 2013). Cretaceous sea levels varied at amplitudes of tens of meters (Miller et al., 2005) and flooded about one-third of the continental areas creating extensive seaways (Ronov et al., 1989; Ronov, 1994).

Oxygen isotopes of marine fossils record the paleotemperature history of the ocean, indicating a cool greenhouse during the Early Cretaceous, warm greenhouse during the middle Cretaceous, and cold greenhouse during the Late Cretaceous (Huber et al., 1995; Barrera and Savin, 1999; Cramer et al., 2009; Friedrich et al., 2012). During the Early and Late Cretaceous the Polar Regions were cool temperate, whereas in the middle Cretaceous the North Polar Region was warm temperate. In contrast, brief glacial episodes have been proposed based on timing and range of sea-level fluctuations (Stoll and Schrag, 2000; Miller et al., 2010), although sedimentologic evidence is inconclusive (Ando et al., 2009). Late Cretaceous paleoclimate is mainly constrained by global-scale ocean current modeling and paleoclimate reconstruction (Pucéat et al., 2005; Haggart et al., 2006; Boucot et al., 2009), by global vegetation simulation (Otto-Bliesner and Upchurch, 1997; Upchurch et al., 1998; Donnadieu et al., 2009; Fricke et al., 2010). Much of our knowledge of the late Cretaceous paleotemperatures has come from marine records (Huber et al., 1995; Barrera and Savin, 1999; Cramer et al., 2009; Friedrich et al., 2012). The terrestrial paleoclimate records are few and the comparison and correlation between marine and terrestrial paleoclimate records are even fewer. A robust comparison among terrestrial and marine records may provide insight into possible similarities and differences in their paleoenvironment and paleoclimate, and help us test ocean-land climate interactions. Additional details on the spatial distribution of paleotemperatures will further resolve the late Cretaceous paleoclimate.

To understand the Cretaceous 'greenhouse' climate, data on magnitudes, rates, and impacts of hydrosphere/atmosphere records, and marine deposits must be integrated with terrestrial sedimentary rocks and fossils. Under the umbrella of International Geosciences Programme (IGCP) 555, the integration of Cretaceous climate data can be achieved by correlating and comparing the long-lived Cretaceous Songliao Basin (SB) in eastern Asia with the Western Interior Seaway (WIS) on the North American plate. The Western Interior Seaway spanned the North American continent dividing it into two landmasses and records Cenomanian to Maastrichtian marine deposition. The Songliao Basin is located on one of the largest landmasses of this period (Fig. 1). A unique, 2400 meter-long core taken by the SKI drilling program (Wang et al., 2008, 2013) recovered the Turonian to Maastrichtian terrestrial record in the SB; it forms the basis for this correlation. Both basins contain significant stratigraphic accumulations and were located within comparable latitudinal ranges (middle latitudes climate zone of the Northern Hemisphere) during the Cretaceous (Fig. 1). Paleomagnetic data show that they were located at middle latitudes similar to where they are now (see Section 2 of this paper). Consequently, correlation and comparison of the continental Songliao Basin with the marine Western Interior Seaway provide an excellent opportunity to study Late Cretaceous climate changes.

In this paper, we review and compare these two important Late Cretaceous basins of East Asia and western North America on opposite sides of the proto-Pacific Ocean and identify similarities and differences in paleoclimate and paleogeographic changes of both regions. This investigation advances understanding of climate change in the Cretaceous greenhouse world, and its relationship to geological events relevant to carbon cycles. It also addresses important problems, such as the identification and timing of important stratigraphic boundaries and the correlation of marine strata with terrestrial strata. Furthermore, this comparison may provide insights for future greenhouse worlds.

2. Late Cretaceous tectonic and paleogeographic settings

During the Late Cretaceous a significant part of the globe was occupied by the proto-Pacific Ocean, which was rimmed by active arc complexes much like today (Fig. 2a). The resultant topography influenced climate and paleoenvironments of adjacent landmasses. In the East Asian region extensive non-marine, rift and back-arc basins and overall low topographic relief were likely related to ongoing subduction to

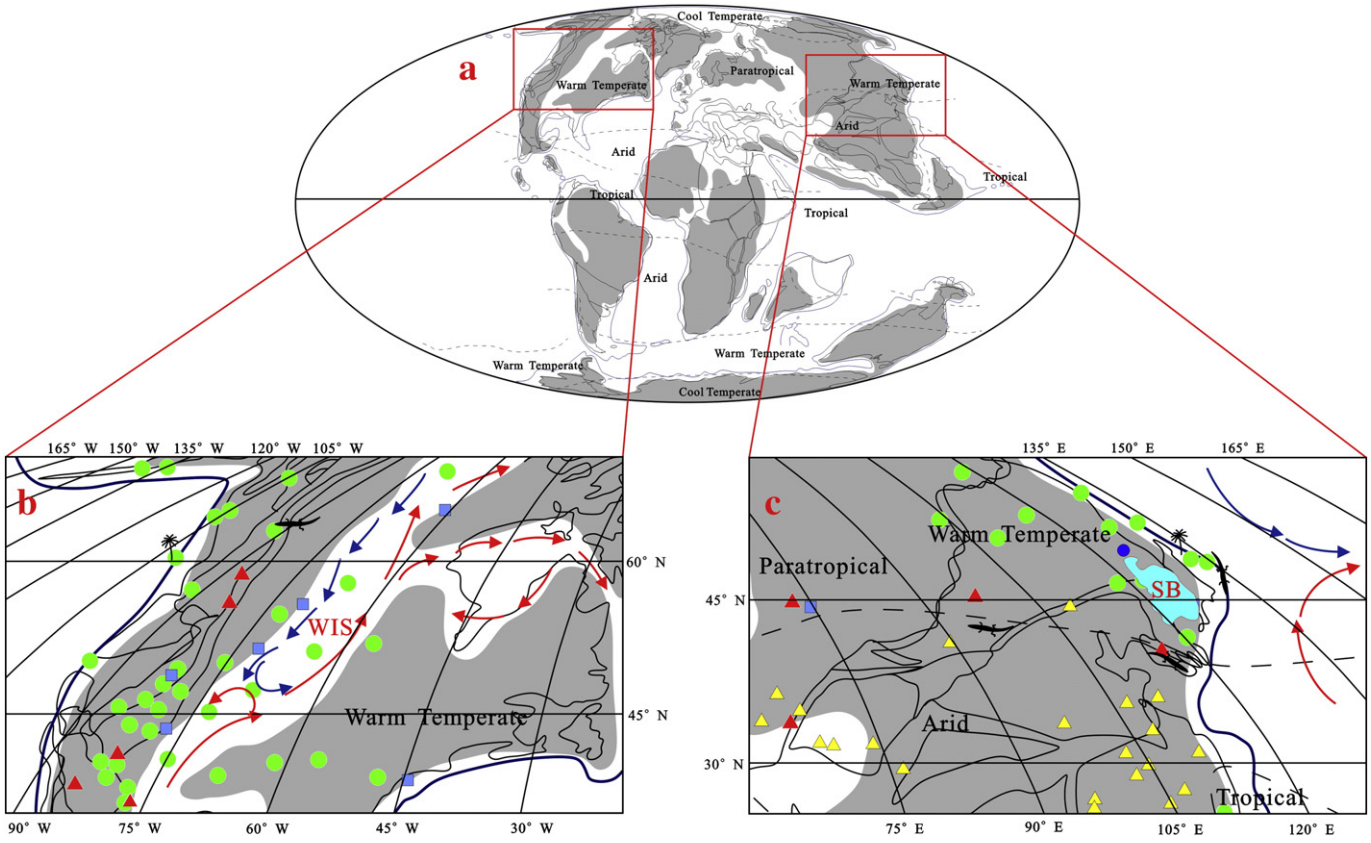

Fig. 1. (a) Map showing the main tectonic plates, paleogeography, and paleoclimate zones of the Earth in the late middle Cretaceous (80 Ma) and location of study area. The paleolatitudes and longitudes, paleogeography and paleoclimatology of (b) North America and (c) East Asia outlined by red boxes. Main ocean paleocurrents: blue arrows indicate south-flowing cool waters; red arrows indicate north-flowing warm waters (after Pucéat et al., 2005; Haggart et al., 2006). Paleoclimate zones are reconstructed from analyses of the distribution of climatologically sensitive deposits: bauxites (blue dots) indicate tropical–subtropical climate, evaporites (yellow triangles) and calcretes (red triangles) indicate arid climate, and coal (green dots) indicates humid climate with widely ranging temperatures. Reptiles ranged from humid to arid climates. SB is the location of the Songliao Basin.
Modified from Boucot et al. (2009).

the east. In western North America, in contrast, the North American plate moved westwards towards the active covergent plate boundary resulting in development of a volumetrically larger and topographically higher orogen than in East Asia (Armstrong and Ward, 1993; Monger, 1993; Haggart et al., 2006). A great variety of Cretaceous basinal and climatic environments are recorded by Cretaceous stratigtraphic successions in the Songliao basin and the Western Interior Basin (Table 1; Fig. 2).

2.1. Songliao Basin

The geologic history of the SB is well known because of extensive drilling for hydrocarbons. The first commercial oil well in Daqing Oil Province was completed in 1959; since then the cumulative oil production is more than 2 billion tons. The modern fault-bounded Songliao Basin is 700 km long from north to south, and 370 km wide from east to west, covering roughly 260,000 km^2 in Heilongjiang, Jilin and Liaoning provinces of NE China (Table 1). Geographically the basin is located between 119°40′~128°24′E, 42°25′~49°23′N. The basin trends in a NNE direction and the basin floor is approximately diamond shaped (Fig. 2c). Coarse terrigenous clastic sediment was delivered from all directions but mainly from the northwest.

North–east Asia, where the Songliao Basin is located, is a complex of discontinuous and amalgamated tectonic plates subdivided by suture zones and fold belts that formed during multiple continental collision events (Fig. 1c) (Şengör and Natal'in, 1996; Yin and Nie, 1996; Hendrix and Davis, 2001). The interior parts of the north–east Asian continent are dominated by non-marine stratigraphic sequences. An extensional rift valley system larger than the Basin and Range province in North America developed in NE China and southern Mongolia from Late Jurassic to Cretaceous time (Fig. 2c) (Graham et al., 1996; Graham et al., 2001; Ren et al., 2002). This rift valley system overlapped onto several interior contractile orogenic zones, leading to three groups of rift basins in the western, central and eastern areas. Cretaceous marine and brackish-water sediments in the three groups of rift basins record five main transgressive interludes from Valanginian to late Santonian (Sha et al., 2008; Xi et al., 2011a). The spatial and temporal distribution of those marine and brackish water intercalations indicate that all transgressions came from the northwestern Paleo-Pacific Ocean (Sha, 2007; Sha et al., 2008). During these transgressions, humid climatic conditions (Wang et al., 2013) produced a number of extensive and long-lasting swamps and marsh lands in both paralic and limnic environments, consistent with low relief across these three basin groups at elevations close to sea level, which enabled regional marine transgression.

South of these rift basins is the North China Craton (NCC), which is separated from the SB by the Yanshan orogenic belt (Fig. 2c). To the north this basin complex is separated from the Siberian Craton (SC) by the Mongolia–Okhotsk suture zone (MOS; Fig. 2c), which formed during the Late Jurassic to Early Cretaceous closure of the Mongol–Okhotsk Sea (Zorin, 1999; Metelkin et al., 2007). To the east, the Japanese Islands are an active offshore magmatic arc separated from mainland Asia by the Sea of Japan, which opened in the Cenozoic via extension (Otofuji, 1996). During Cretaceous time, however, Japan was situated appreciably closer to the Asian continental region than it is today.

Paleomagnetic data show that the North China plate, the Yangtze plate and the Korean plate united to form a single block beginning in Late Jurassic (Gilder and Courtillot, 1997). Paleomagnetic studies of fifty-five Cretaceous lavas indicate that this area did not move relative

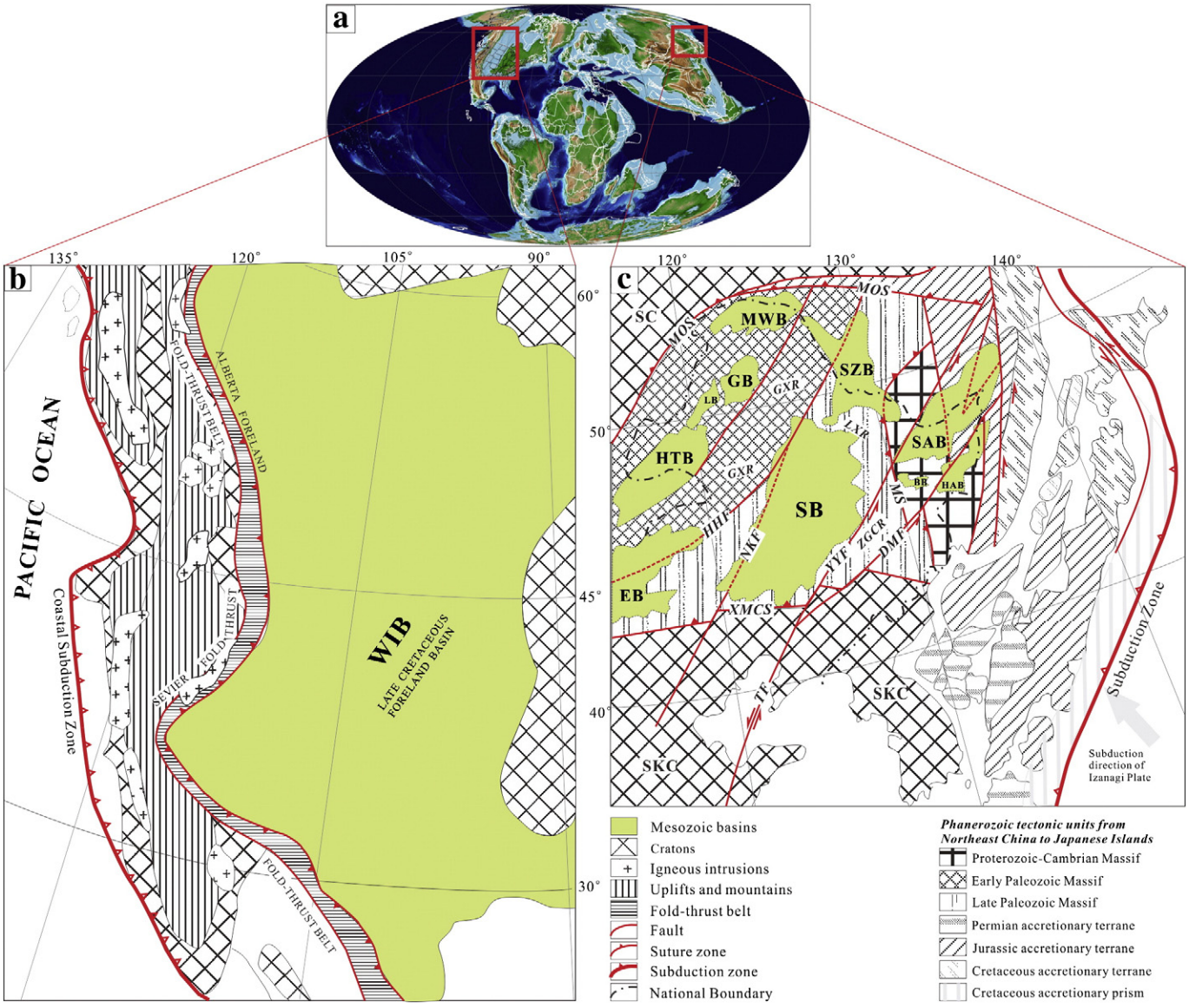

Fig. 2. Generalized paleogeographic maps of the Late Cretaceous Western Interior Basin and Songliao Basin. (a) Late Cretaceous global paleogeographic map after Scotese (2002). (b) Late Cretaceous paleogeographic map of Western Interior Basin modified after Kauffman and Caldwell (1993) and Schwans (1995). (c) Late Cretaceous paleogeographic map of Songliao Basin modified after Ren et al. (2002), Golozubov et al. (2006), and Zhang et al. (2006). Position of Japanese islands are restored for 85 ~ 95 Ma modified after Ishida et al. (2003) and Golozubov et al. (2006). MOS: Mongolia–Okhotsk suture zone; HHF: Hegenshan–Heihe Fault; NKF: Nenjiang–Kailu Fault; MS: Mudanjiang suture zone; YYF: Yilan–Yitong Fault; DMF: Dunhua–Mishan Fault; XMCS: Xra–Muron–Changchun suture zone; TF: Tanlu Fault. SC: Siberia Craton; SKC: Sino–Korean Craton. WIB: Western Interior Basin; SB: Songliao Basin; MWB: Mohe–Wusumeng Basin; GB: Genhe Basin; LB: Labudalin Basin; HTB: Hailar–Tamuchage Basin; SZB: Sunwu–Zeya Basin; SAB: Sanjiang–Amour Basin; HAB: Hulin–Aerchang Basin; EB: Eren Basin; BB: Boli Basin. GXR: Great Xing'an Range; ZGCR: Zhangguangcai Range; LXR: Lesser Xing'an Range.

to Eurasia (Zhu et al., 2002), which suggests that the Songliao Basin including the western and the eastern rift basins were located at middle latitudes similar to where they are now.

Table 1
Comparison of key properties of the Songliao Basin and Western Interior Basin.[a]

Property	Songliao Basin	Western Interior
Maximum dimensions	360 × 820 km	1200 × 5000 km
Aerial extent	260,000 km2	6,000,000 km^2
Latitudinal span	40°N to 50°N	33°N to 70°N
Tectonic setting	Rift Basin	Foreland Basin
Beginning age	Late Jurassic	Middle Jurassic
Ending age	Paleocene	Eocene
Maximum thickness	9847 m	7800 m
Main source rock age	M. Turonian and L. Santonian	Turonian–Santonian

[a] Modified from Kauffman and Caldwell (1993) and Cook and Bally (1975).

2.2. Western Interior Basin

The Western Interior Basin was about 1200 km wide at its widest point from southwestern Utah to eastern Kansas during the Turonian and Coniacian stages and more than 5000 km long from central New Mexico to Alaska, an area more than 6,000,000 km^2, nearly 23 times the size of the SB (Table 1; Fig. 2b). The Western Interior Seaway (WIS) has been studied over a period of nearly 200 years documenting the stratigraphy, biostratigraphy, magnetostratigraphy, chemostratigraphy, and climate modeling constrained by numerous radiometric dates (Obradovich, 1993).

Strata of the Cretaceous Western Interior Seaway (WIS) of North America were deposited within a retroarc foreland basin relative to the generally north–south oriented Andean style Cordilleran margin (e.g., Dickinson and Snyder, 1978; Fig. 2b). As the foreland fold–thrust system propagated eastward through the Late Cretaceous, a family of principal thrusts accomplished much of the shortening. In a pattern

typical for foreland systems, these thrusts generally propagate in-sequence craton-ward, each typically active for a few million years, before being supplanted by a younger thrust (e.g., Royse et al., 1975; Gardner, 1995). The advance of each thrust is clearly recorded by an associated coarse clastic sediment wedge of fluvial-alluvial strata reflecting uplift and erosion of the older strata, as well as load-driven accommodation for the sediment wedge (Royse et al., 1975; Lawton, 1986).

Deformation of older thrust-proximal alluvial strata into progressive unconformities also elucidates the timing of thrust advances (e.g., DeCelles et al., 1995). Sediment provenance studies demonstrate the progressive addition of older recycled material into the thrust-proximal foreland with the advance of each thrust sheet (DeCelles et al., 1995). Each thrust-related sediment wedge can be traced through alluvial to fluvial to shoreline facies eastward toward the main foreland (e.g., Gill and Cobban, 1966). The eastward facies succession is nowhere better continuously traceable than from the Wasatch Mountains eastward around the Book Cliffs of Utah and into western Colorado. Because of the relationship to individual propagating thrusts, the shoreline stratigraphy of the Western Cretaceous Interior Seaway has a markedly cyclic character, well known because of the economic coal deposits associated with the coastal plain facies (Gardner, 1995; Jordan, 1995; Schwans, 1995). Although facies patterns vary in detail with latitude along western WIS shoreline (Gardner, 1995; Schwans, 1995), a similar tempo of clastic wedge advances is tied to fold–thrust belt evolution.

These structural–stratigraphic relations foster the view that cyclic shoreline Upper Cretaceous stratigraphy along an east–west transect through Utah and Colorado principally reflects tectonic drivers that facilitated subsidence and sediment supply. Nevertheless, some workers in the Book Cliffs section have alluded to eustasy as a driver for the long-term development of cyclic shoreline stratigraphy, based on correlation of cycles to published sea-level curves (e.g., Van Wagoner et al., 1990; DeCelles and Giles, 1996). Determining the relative roles of tectonically driven uplift and subsidence (accommodation), climate, sediment supply, and eustasy in the development of the stratigraphic architecture of the Sevier retro-foreland basin remains a topic of lively debate and the subject of computational modeling of the basin foreland (as well as foreland basins in general) (e.g., Jordan, 1995). In any event, these combined drivers produced the stratigraphic template against which global oceanographic and atmospheric change, registered in paleontologic, elemental and isotopic proxies are preserved in the strata of the Cretaceous Interior Seaway.

The withdrawal of the Cretaceous Interior Seaway and establishment of regionally extensive non-marine depositional systems during the later part of the Cretaceous in the U.S. segment of the Sevier retroarc foreland basin broadly coincided with the change from thin-skinned thrusting to basement-involved (thick-skinned) shortening in the modern Rocky Mountain region (e.g., Graham et al., 1987; DeCelles, 1994). This change in structural style converted the formerly expansive Sevier foreland basin into a 'broken foreland' composed of contractile block uplifts and intervening relatively small non-marine basins (Jordan, 1995). The advent of this tectono-topographic change heralded the onset of the Laramide orogenic phase of foreland evolution, and has been widely regarded as reflecting the shoaling angle of the subducting slab (Dickinson and Snyder, 1978).

3. Chronostratigraphic records

Chronostratigraphic correlation of the Cretaceous record of the East Asian Songliao Basin (SB) with the North American Western Interior Seaway (WIS) is essential in order to compare Cretaceous climate data in these two epicontinental basins. Timing and rates of atmosphere/hydrosphere interactions in large confined basins can be tested. Chronostratigraphic correlation of these basins is based on radiometric ages, magnetochrons, and limited biota shared by both paleobiogeographic provinces. However, the largely non-marine biota of the SB differs from the marine biota of the WIS. Numerical ages of both the non-marine biota of the SB and the marine biota of the WIS have been interpolated by the quantitative graphic correlation method, thereby, enabling testable correlation hypotheses and projection of stage boundaries from global reference sections (Scott et al., 1998; Scott, 2009; Scott et al., 2012).

3.1. Songliao Basin

The first scientific core in the Songliao Basin (SB), SKI, was drilled during 2007–2008 (Wang et al., 2008). This core provides the most continuous Upper Cretaceous geological record in northeast Asia up to now. The SKI core intersects the stratigraphic section in ascending order from the Quantou, Qingshankou, Yaojia, Nenjiang, Sifangtai, and Mingshui Formations (Fig. 3) (Sha, 2007; Wan et al., 2013). A detailed, high-precision biostratigraphic zonation of the cored section is based on diverse and abundant microfossil assemblages: 20 ostracode assemblages, 10 phytoplankton assemblages, 7 palynological zones, and 4 charophyte assemblages. In addition, a low diversity marine foraminiferal assemblage was recently discovered in the Nenjiang Formation (Xi et al., 2011b). These bioevents have been calibrated to numerical ages (Scott et al., 2012; Wan et al., 2013).

The chronostratigraphic framework of the SKI composited core is constrained by high quality SIMS U–Pb zircon radiometric ages and by magnetostratigraphy. Four $^{206}Pb/^{238}U$ ages of 91.4 ± 0.4 Ma, 90.1 ± 0.4 Ma, 90.4 ± 0.6 Ma, and 83.7 ± 0.5 Ma were determined (Deng et al., 2013). Eleven local magnetozones have been identified as Chrons C34N to C28N (Deng et al., 2013). The zones are assigned to the Upper Cretaceous stages by correlation with zones in central Asia, Europe and North America. At the base of the core the upper part of the Quantou Formation is Turonian; the Qingshankou Formation is uppermost Turonian–lower Coniacian; the Yaojia Formation spans from upper Coniacian to middle Santonian; the Nenjiang Formation is upper Santonian to middle Campanian; the Sifangtai Formation is limited to upper Campanian; and the Mingshui Formation is uppermost Campanian to Maastrichtian and spans the K/Pg boundary extending into the Paleocene Series.

3.2. Western Interior Basin

Cretaceous sedimentary rocks in the Western Interior Basin are well exposed and onlap Upper Jurassic and older strata. The Albian to Campanian section is continuously cored in numerous wells (Dean and Arthur, 1998a), and the Campanian–Maastrichtian interval is known from outcrops. The thickness of the Upper Cretaceous section varies across the basin because of local tectonic features and is more than 1524 m (5000 ft) thick in reference sections (Cobban et al., 2006). The stratigraphic section is dominantly siliciclastics with interbedded limestone, chalk, and marl in the basin center (Kauffman and Caldwell, 1993).

The Upper Cretaceous section is very fossiliferous yielding ammonites, inoceramids, planktic and benthic foraminifera, calcareous nannofossils, dinoflagellates, spore and pollen, and diverse vertebrates. Ammonites are the primary tool for dividing the section into biozones (Fig. 3) (Cobban, 1993; Hancock et al., 1993; Kauffman et al., 1993; Cobban et al., 2006). The base of the Upper Cretaceous at the Albian–Cenomanian boundary correlates with the top of the Mowry Formation in Wyoming and the Clay Spur Bentonite Bed dated at 97.88 ± 0.69 Ma (Obradovich, 1993; Ogg et al., 2012). The Cenomanian–Turonian boundary is in the upper part of the Greenhorn Formation (Scott et al., 1998). The Turonian–Coniacian boundary is in the basal part of the Niobrara Formation (Walaszczyk and Cobban, 2000; Hancock and Walaszczyk, 2004). The Coniacian–Santonian boundary is in the upper part of the Niobrara Formation (Walaszczyk and Cobban, 2007). The

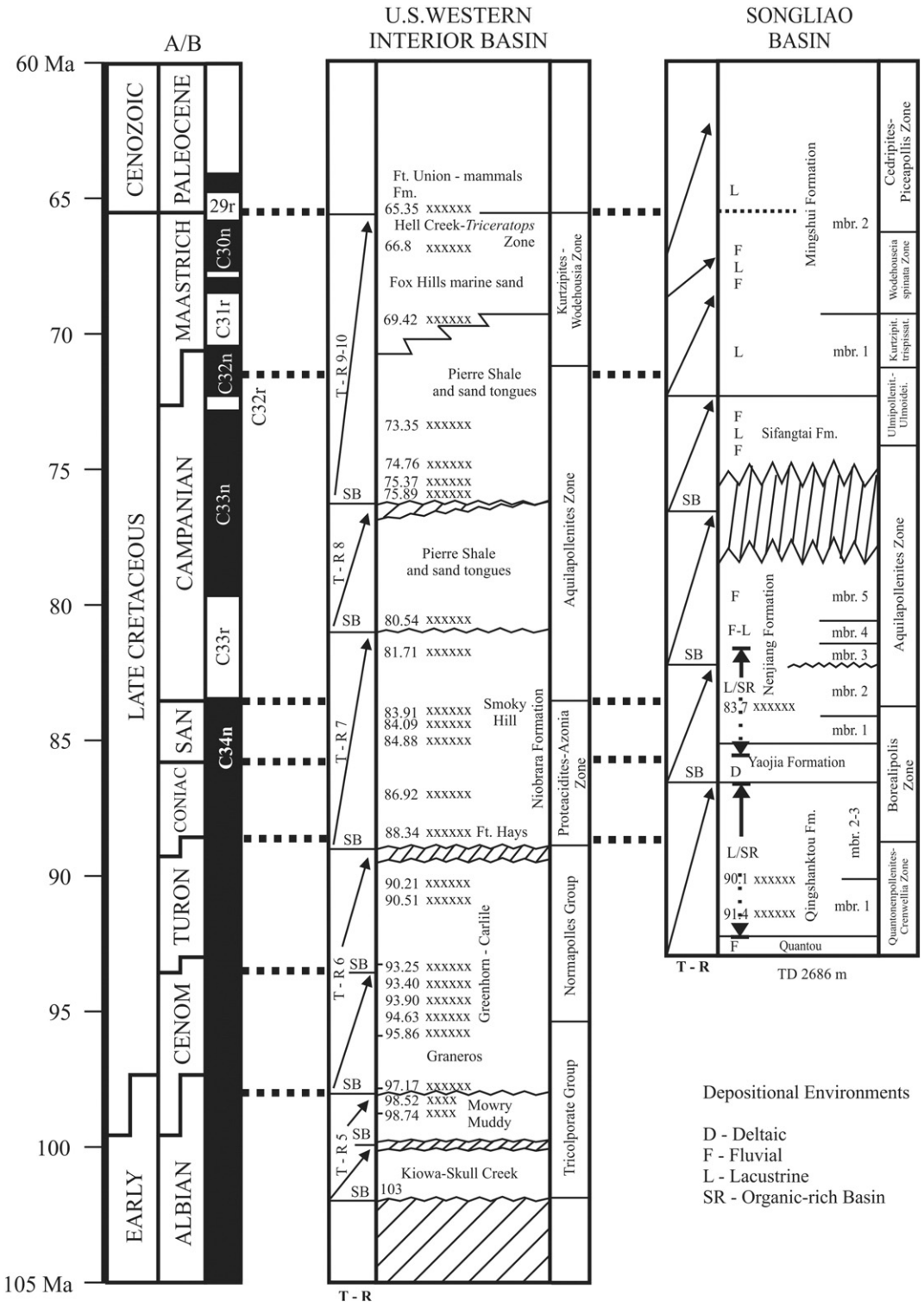

Fig. 3. Correlation of Upper Cretaceous stratigraphy between Western Interior and Songliao Basin. A/B: Two age models of Upper Cretaceous stages: A. Ogg et al. (2004) and Scott (2009). Western Interior transgressive–regressive (T–R sequences by Kauffman (1977, 1984)); those in Songliao Basin by P.J. Wang et al. (2009). Radiometrically dated bentonite or tuff beds indicated by 'xxx' in Western Interior (Obradovich, 1993) and in Songliao Basin (He et al., 2012).

Santonian–Campanian boundary in the WIS is in the upper part of the Smoky Hill Member of the Niobrara Formation (Cobban et al., 2006). The Campanian–Maastrichtian boundary in the WIS is in the basinal marine Pierre Shale. The Maastrichtian–Paleogene boundary is defined in non-marine fluvial strata in the uppermost part of the Hell Creek Formation in Montana (Smit and van der Kaars, 1984) and the Lance Formation in Wyoming (Bohor et al., 1987).

The numerical age of the WIS section is well constrained by $^{40}Ar/^{39}Ar$ dates of sanidine and zircon in numerous bentonites (Fig. 3; Obradovich, 1993; Ogg et al., 2012). These ages are the pinning points for the

interpolation of ages for the biozones (Cobban et al., 2006). Latest Cretaceous magnetochrons C31R through C33N are also integrated with bentonite ages (Hicks et al., 1999). A strontium isotope curve of Western Interior fossils correlates with European data and projects stage boundaries into the WIS ammonite zones (McArthur et al, 1994).

3.3. Comparison and discussion

The Songliao Basin section correlates with the Western Interior Seaway Upper Cretaceous section by radiometric ages, magnetochrons, pollen zones, and planktic foraminifera (Fig. 3). Three Campanian–Maastrichtian pollen assemblage zones in the SKI are also in the WIS: *Aquilapollenites*, *Kurtzipites trispissatus*, and *Wodehousia spinata* (Nichols and Sweet, 1993). These zones correlate the Pierre Shale, Fox Hills Formation and the several overlying formations in the WIS with members 3–5 in the upper part of the Nenjiang, the Sifangtai, and part of the Mingshui Formations in the Songliao Basin.

In the SKI the Santonian/Campanian boundary is identified by the boundary of Chrons C33R and 34N and the *Aquilapollenites* zone in member 2 of the Nenjiang Formation. In the WIS the base of the Campanian is correlated with the *Scaphites leei* III ammonite zone and the Sr isotope ratio of 0.707457 ± 16 in the upper part of the Smoky Hill Member of the Niobrara Formation (McArthur et al., 1994; Cobban et al., 2006). The base of the Maastichtian Stage in the SKI core is identified by the base of the *Kurtzipites trispissatus* zone and the Maastrichtian/Danian boundary is placed within the base of Chron C29R and the top of the *Wodehouseia spinata* zone.

4. Lacustrine and marine cyclostratigraphy: base-level, eustatic and climatic cycles

Base-level cycles are driven either by relative sea level or by basinal tectonic changes. In marine basins eustasy alters accommodation space as sea level rises and falls. In intra-continental basins tectonics drive both basin subsidence and depositional cycles. The Songliao Basin was isolated from the ocean except for two brief periods in the late Turonian of the Qingshankou Formation and in the early Campanian in the lower part of the Nenjiang Formation (Xi et al., 2011a).

Paleoclimate research has shown that astronomical forcing drove global climate change in the Earth's history and may be recorded in both continental and marine sedimentary strata (Hinnov and Hilgen, 2012). The orbitally forced cycles are recorded in Cretaceous marine successions around the world (e.g., Locklair and Sageman, 2008; Lanci et al., 2010; Husson et al., 2011), and are one calibration tool of the Cretaceous time scale (Ogg et al., 2012). Late Cretaceous sedimentary cycles in the WIS have been studied extensively (Sageman et al., 1997; Gale et al., 2008; Locklair and Sageman, 2008), and Milankovitch cycles were recently identified in Late Cretaceous terrestrial strata in the SB (Wu et al., 2009, 2013). It may be possible to correlate Milankovitch cycles between the two basins once comparable high-precision geochronology points or framework were obtained, such as high-resolution U–Pb, Ar–Ar ages and magnetostratigraphy (e.g., Meyers et al., 2012; Deng et al., 2013 and see Section 3).

4.1. Songliao Basin

4.1.1. Base-level and eustatic cycles

High-resolution sequence stratigraphy of the Upper Cretaceous section cored in the SKI (Fig. 4) was based on centimeter-by-centimeter description integrated with well-logs, seismic data and well-to-well correlation in the SB (Cheng et al., 2009; G.D. Wang et al., 2009; Gao et al., 2009; P.J. Wang et al., 2009). Two sequence contacts in the core are correlated with regional seismic horizons T_{07} to T_{03}. The Quantou Formation to the top of the Nenjiang Formation composes the oldest second-order Turonian–Campanian sequence, although its base was not cored. This sequence is composed of smaller scale cycles of fining-upward and coarsening-upward sets. Its basal sedimentary facies represents a fluvial environment grading up into alternating lake-delta to marine, to lake, finally back to fluvial facies. Red beds in two stratigraphic intervals were dated at about 92 Ma to 91.4 Ma and 86.1 Ma to 84.5 Ma, respectively, and the maximum flooding interval is dark gray, organic-rich shale in members 1 and 2 of the Nenjiang Formation. These intervals suggest a relatively warm dry climate during these periods in the region. According to the color and organic content of the sediments, some time periods during the first second-order sequence were generally humid and the most humid climate apparently was during 84.5 Ma to 81 Ma. The second second-order sequence includes the Sifangtai Formation and the Mingshui Formation, uppermost Campanian (79 Ma) to Danian (64.0 Ma). This sequence is composed of a series of fining up cycles and alternating fluvial–lacustrine facies. The maximum flooding interval is shale and sandstone in member 1 of the Mingshui.

Six third-order sequences cycles are composed of fining-upward followed by coarsening-upward facies. The third-order cycles are from 590 m to 106 m thick undecompacted and the durations averaged about 4.5 myr. The depositional environments of third-order cycles begin with fluvial facies followed by lake then back to fluvial or delta facies. The boundary at the top of the lowest sequence is the top of deltaic sandstone. The top of the second sequence marks the beginning of basin deepening at the contact between sandstone and the dark gray, organic-rich shale of the first member of the Nenjiang Formation. A marine flooding interval was recognized in the middle interval of the 3rd sequence in members 1 (K_2n^1) and 2 (K_2n^2) of the Nenjiang (Fig. 4; Wang et al., 1995; Xi et al., 2011a). The top of the third third-order sequence is the boundary between members 3 and 4 of the Nenjiang in a sandstone interval, which is seismic reflector T_{04}. The fourth third-order sequence ranges from uppermost Santonian to lower Campanian and the maximum lacustrine flooding interval is shale member 4 of the Nenjiang. The fifth third-order sequence spans the entire Sifangtai Formation; its base is a regional erosion contact and its top is the base of the Mingshui Formation and the contact between fluvial facies and the lacustrine facies that indicate deepening. The sixth third-order sequence spans the entire Mingshui Formation.

4.1.2. Milankovitch cycles

Meter-scale sedimentary cycles are definable and well developed throughout the SKI south core (Cheng et al., 2008, 2009; G.D. Wang et al., 2009; Gao et al., 2009; P.J. Wang et al., 2009). The cycles were recorded by variations in rock color, lithology and facies, which show normal graded, reverse graded and non-graded cycles (Cheng et al., 2008). The thicknesses of these meter-scale cycles range from 0.5 m to 1.5 m, but in the Quantou Formation thicknesses are up to 6.5 m. Fisher plots indicated that the basic meter-scale cycles could be bundled into the fifth and fourth order cycles with 1:3–4 and 1:6–12 ratios, respectively. These different order cycles are attributed to Milankovitch cycles of precession, and short and long eccentricity frequencies (Cheng et al., 2008).

Time-series methods were conducted on the paleoclimate proxies of natural gamma-ray (GR), thorium (Th) log data and magnetic susceptibility (MS) in order to further define Milankovitch cycles. Spectral and wavelet analyses on the natural gamma-ray logs of 10 wells of the Qingshankou Formation from different tectonic units reveal orbital cycles of precession (20 kyr), obliquity (38 kyr), and eccentricity (100 kyr and 405 kyr), providing strong evidence for astronomically driven climate changes in the Late Cretaceous terrestrial environments (Wu et al., 2009). Cyclostratigraphic analyses on the Quantou, Qingshankou, Yaojia, and Nenjiang Formations in the SKI south well confirmed the excellent preservation of astronomically driven sedimentary cycles, including long and short eccentricity, obliquity, and precession cycles constrained by four high-resolution SIMS U–Pb zircon ages (He et al., 2012; Wu et al., 2013) (Fig. 5).

The sedimentary cycles recorded by the GR and Th logs, and MS of the relatively homogeneous, fine-grained mudstones in the Qingshankou and

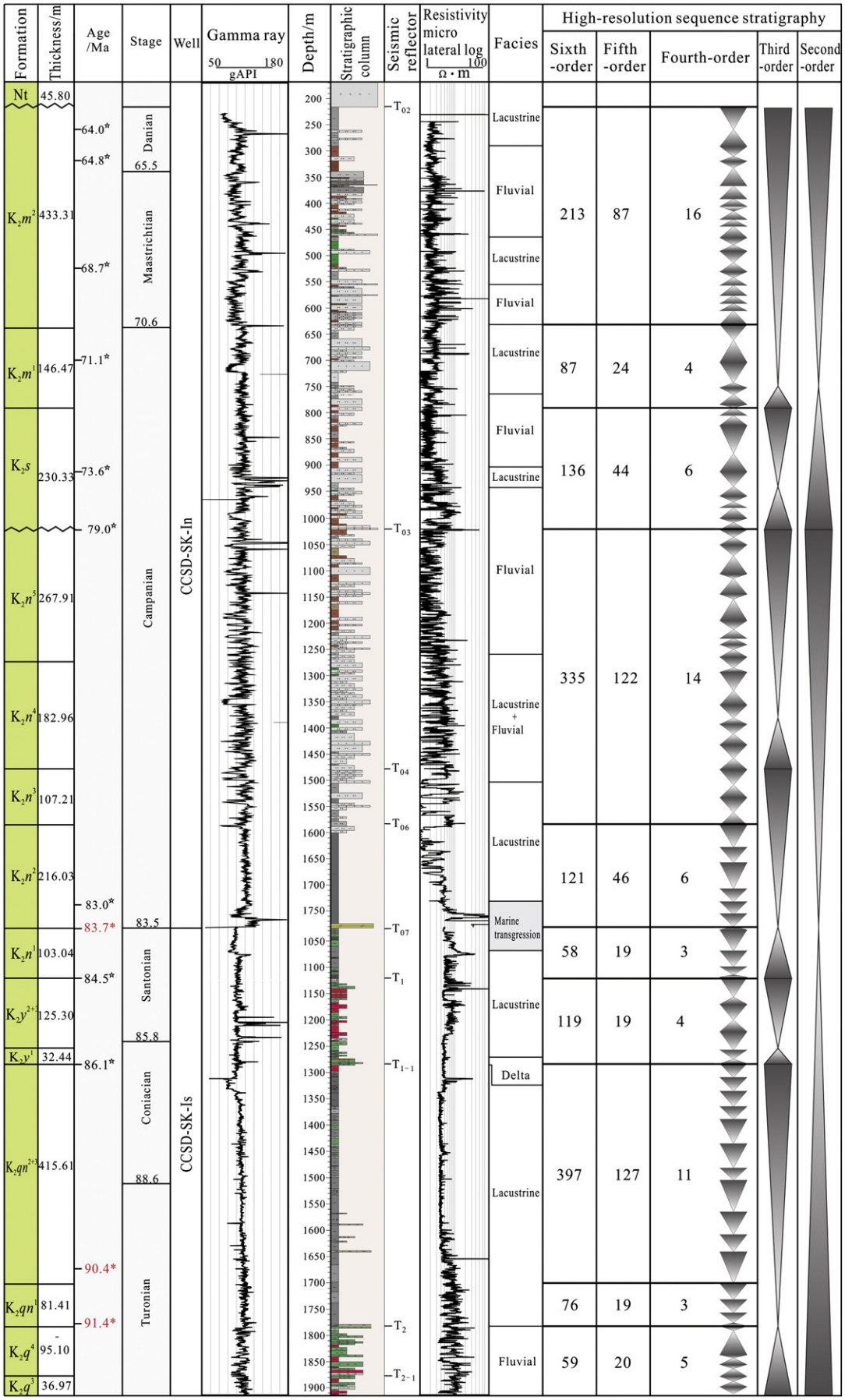

☆–Paleomagnetic interpolated ages； *–SIMS zircon U-Pb ages

Nenjiang Formations may reflect changes in runoff in response to wet/dry periods as predicted by paleoclimate simulations (Sewall et al., 2007; Chen et al., 2013). Wet periods may have enhanced chemical weathering and clay and magnetic minerals inputs, resulting in high values, while decreased chemical weathering during dry periods may correspond to the negative peaks (Wu et al., 2009; Li et al., 2013).

Cyclostratigraphic analysis showed that the SKI south core recorded about 89 short eccentricity and about 22 long eccentricity sedimentary cycles, respectively (Wu et al., 2013) (Fig. 5), and the extracted 405-kyr long eccentricity cycles were tuned to the theoretical long eccentricity cycles of astronomical solutions La2010 provided by Laskar et al. (2011). The established astronomical time scale (ATS) with age uncertainly of 0.09 Ma induced by astronomical solutions (Laskar et al., 2011) showed that the age of the SKI south well ranged from lower Turonian to lower Campanian, and predicted the ages and durations of geological events (Fig. 5). The age of the polarity boundary of C33r/C34n is estimated as 83.63 Ma, which is 0.37 Ma younger than that of the Geological Time Scale 2004 (Gradstein et al., 2004), and is consistent with the age of 83.64 Ma given by Ogg (2012). The ages and durations of the three short reverse polarities recorded in the second member of the Yaojia Formation are 84.82–84.86 Ma (40 kyr), 84.98–85.09 Ma (110 kyr), and 85.24–85.63 Ma (39 kyr) (Fig. 5). This 'absolute' ATS provides a precise numerical time scale for correlation of strata and events between marine and terrestrial systems.

4.2. Western Interior Basin

4.2.1. Base-level and eustatic cycles

The Albian–Maastrichtian stratigraphic succession in the Western Interior is composed of six second-order transgressive–regressive cycles approximately six to eight myr in duration (Kauffman, 1984) (Fig. 6). These six sequences record times during which North America was divided into eastern and western landmasses by a seaway connecting the southern Tethyan Sea with the northern Boreal Sea. The basal contacts of these sequences are fluvial erosion surfaces, marine basin calcarenite beds or marine condensed intervals. The basin margin sequences are composed of fluvial–deltaic and shoreface sandstones that grade basinward into pelagic shale and cyclically interbedded marl and limestone.

The second-order transgressive–regressive sequences are composed of third-order sequences averaging 2–3 myr in duration (Fig. 6). The Upper Albian short-term sequences are flooding successions of nearshore sandstone and lagoonal to offshore shale (Scott et al., 1998; Holbrook et al., 2006; Oboh-Ikuenobe et al., 2007). The offshore Cenomanian–Turonian sequence boundaries are delineated between regressive prodeltaic and shoreface sands and silts overlain by carbonate-rich mud rocks (Leithold, 1994; Leithold and Dean, 1998; Gale et al., 2008). The western onshore Cenomanian–Turonian sequences have sharp erosional diastems that separate regressive laterally persistent sandstone and siltstone below from transgressive lenticular sandstone lithosomes above (Nummedal et al., 1993). The Coniacian–Santonian sequences are composed of transgressive mud rocks grading up into progradational nearshore and offshore sand (Allen and Johnson, 2011).

On the western shore Campanian–Maastrichtian third-order sequences are transgressive-progradational sand bodies that are composed of fourth-order cycles. A Lower Campanian third-order sequence has been interpreted as composed of "shelf sand ridge complexes to lowstand shorefaces to tide dominated deltas" (Painter, 2009). During sea-level fall shoreface processes eroded into older shoreface and shelf deposits. Six transgressive facies overlie progradational shoreface sand bodies that incise into the underlying sands (Bergman and Walker, 1999). The subsequent transgression deposited shell lags and phosphate pebbles on top of the shoreface sands. The estimated durations of each short-term T–R cycle is about 167 kyr and relative sea level fluctuated up to 50–60 m; local tectonics may have been the controlling process. The amplitudes, frequencies and correlation of WIS basin-scale unconformities with global Campanian–Maastrichtian unconformities need to be tested.

4.2.2. Milankovitch cycles

Small-scale depositional cycles at the Milankovich climatic frequencies are well documented in WIS (Fig. 7). In the center of the basin in Colorado, Middle Cenomanian to Lower Turonian 405 kyr eccentricity packages of winnowed to condensed carbonates and shaley facies are correlated with similar cycles in Europe and India (Gale et al., 2002, 2008). The winnowed and condensed parts of the 1–5 meter-thick packages are trangressive limestones or calcarenite tempestites, and the cycles are correlated by biostratigraphic and chemostratigraphic frameworks with retrograding to prograding sandstones on the western shore (Sageman, 1985; Gale et al., 2008).

Shorter-term decameter to decimeter Milankovitch cycles are rhythmically interbedded limestone–marlstone couplets. These cycles are well developed in the Cenomanian–Turonian Greenhorn Formation (Sageman et al., 1997) and in the Turonian–Campanian Niobrara Formation (Dean and Arthur, 1998b; Locklair and Sageman, 2008). Bedding couplets in the Bridge Creek Member of the Greenhorn were attributed to Milankovitch cycles of the precession, obliquity and eccentricity frequencies by spectral analysis (Fig. 7; Arthur et al., 1984; Eicher and Diner, 1989; Sageman et al., 1997). These cyclic deposits are the product of complex interacting factors in which insolation variations lead to wet/dry runoff cycles and dilution/redox marine cycles that altered biotic carbonate productivity and siliciclastic dilution (Sageman et al., 1997, 1998; Locklair and Sageman, 2008). Bedding cycles in the Fort Hays Member of the Niobrara can be traced for many kilometers as stratigraphic marker beds and represent precession, obliquity and eccentricity frequencies (Fig. 7; Hattin, 1971; LaFerriere et al., 1987; Laferriere, 1992; Locklair and Sageman, 2008).

Cyclostratigraphic techniques measure the duration of a rhythmically bedded interval that preserve climate cycles at levels of resolution far exceeding most radio-isotopic dating tools. Using bandpass filtering techniques, the duration of the Bridge Creek Limestone Member of the Greenhorn Formation is estimated at about 1.52 myr, a value that is supported by recent radio-isotope dating studies (Sageman et al., 2006; Meyers et al., 2012). This duration would equate to about fifteen 100 kyr eccentricity cycles, about thirty-eight 40–42 kyr obliquity cycles, and about seventy-six 20 kyr precession cycles.

The gamma ray log of the Bridge Creek in a core in the central WIS is divided into thirteen marl–limestone cycles 1 to 3 m thick that are interpreted to reflect an eccentricity frequency (Scott et al., 1998). The limestone–marl cycles in the Fort Hays Member of the Niobrara Formation are 2.4 to 5.8 m thick and appear to represent the eccentricity frequency also (Dean and Arthur, 1998a; Scott et al., 1998; Locklair and Sageman, 2008). The durations of the Coniacian and Santonian stages were estimated at 3.40 ± 0.13 myr and 2.39 ± 0.15 myr, respectively (Locklair and Sageman, 2008).

4.3. Comparison and discussion

Sedimentary cycles of eccentricity, obliquity and precession bands are present in both the SB and WIS basins, which provide overwhelming evidence that orbital forcing played an important role in global climate change in the Late Cretaceous greenhouse and is recorded in both

Fig. 4. High-resolution sequence stratigraphy of Upper Cretaceous in Songliao Basin, based on centimeter-by-centimeter description of the SKI coupled with well-logs and paleoenvironmental interpretations. Upper Cretaceous of the SB can be subdivided into sequences of 2 second-order, 6 third-order, 72 fourth-order, 527 fifth-order and 1601 sixth-order. The figure on the right side of each segment is the number of cycles in each member or formation.
Modified from Gao et al. (2009).

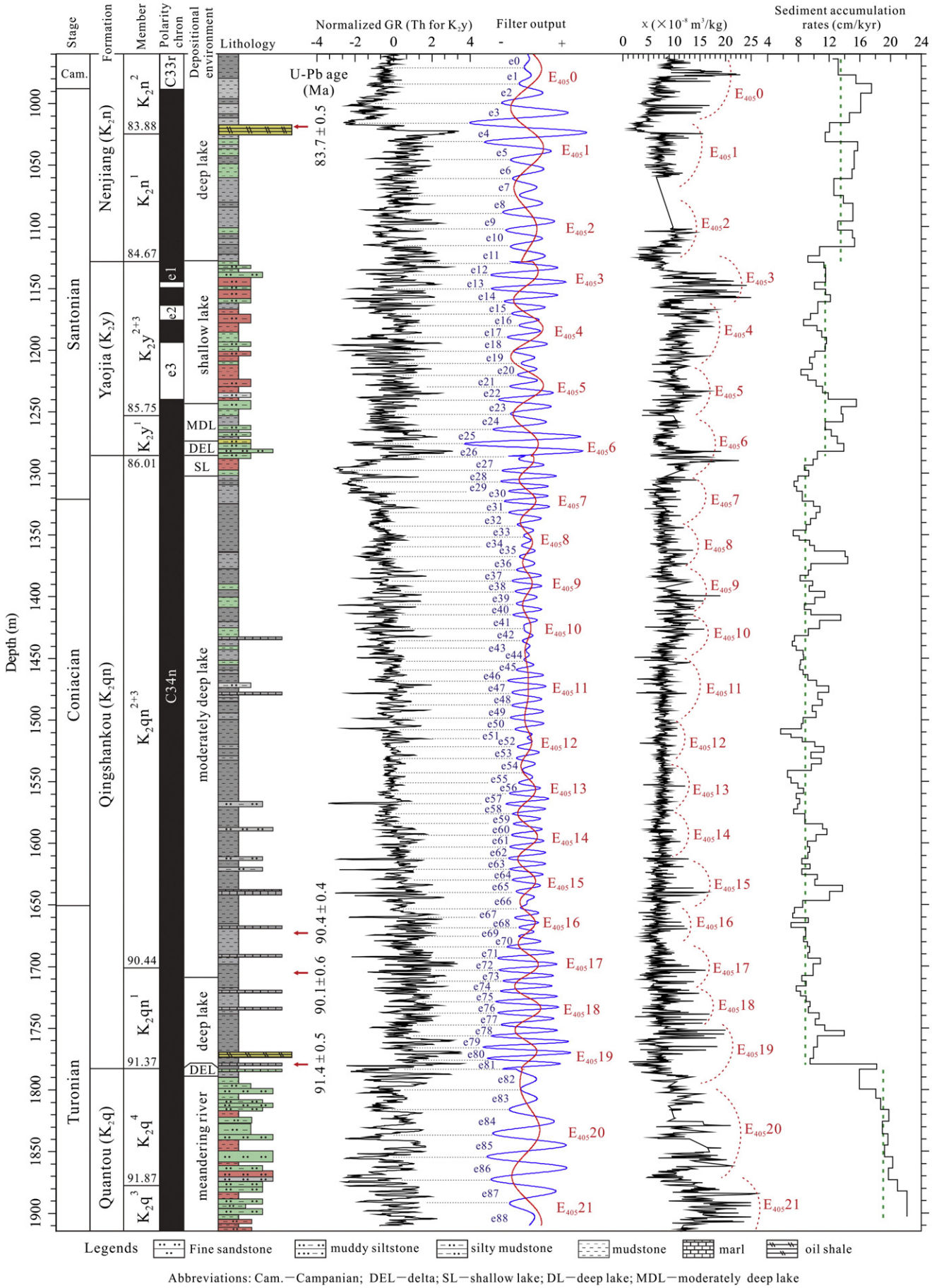
Stage
Formation
Member
Polarity chron
Depositional environment
Lithology
Normalized GR (Th for K2y)
Filter output
x (×10⁻⁸ m³/kg)
Sediment accumulation rates (cm/kyr)
U-Pb age (Ma)
Depth (m)
Cam.
Santonian
Coniacian
Turonian
Nenjiang (K2n)
Yaojia (K2y)
Qingshankou (K2qn)
Quantou (K2q)
C33r
C34n
e1
e2
e3
deep lake
shallow lake
moderately deep lake
meandering river
MDL
DEL
SL
83.88
84.67
85.75
86.01
90.44
91.37
91.87
83.7 ± 0.5
90.4 ± 0.4
90.1 ± 0.6
91.4 ± 0.5
Legends
Fine sandstone
muddy siltstone
silty mudstone
mudstone
marl
oil shale
Abbreviations: Cam.—Campanian; DEL—delta; SL—shallow lake; DL—deep lake; MDL—moderately deep lake

marine and continental environments (e.g., Sageman et al., 2006; Gale et al., 2008; Locklair and Sageman, 2008; Wu et al., 2009, 2013). The identification of the most stable 405 kyr eccentricity cycles opened a unique window for high-resolution correlation between marine and continental strata and major geological events (Figs. 5 and 7).

The response of sedimentary cycles to orbital forcing varied between different depositional environments. In the SB the precession cycles are significant in fluvial facies of the Quantou Formation and in deltaic and shallow lacustrine facies of the Yaojia Formation. In contrast, eccentricity cycles are well developed in the deep lacustrine facies of the Qingshankou and Nenjiang Formations. However, the records of obliquity cycles are relatively weak in all facies (Wu et al., 2009, 2013). In the WIS rhythmically interbedded decameter to decimeter limestone–marlstone eccentricity cycles are well developed in the Cenomanian–Turonian Greenhorn Formation (Sageman et al., 2006; Gale et al., 2008). Limestone bedding cycles in the Fort Hays Member of the Niobrara represent precession, obliquity and eccentricity frequencies (Locklair and Sageman, 2008). The sedimentary cycles in the WIS and SB are interpreted to be controlled by wet/dry runoff cycles, and orbital forcing controlled the siliciclastic dilution cycles in marine environments of the WIS.

Long-period orbital cycles may play an important role in Cretaceous global climate change but the mechanism still remains largely unknown. In the SB, besides the short period (<405 kyr) Milankovitch cycles, the ~1.0 myr and 2.34 myr long-period eccentricity cycles and 1.2 myr long obliquity cycles were detected in the non-marine sequences (Fig. 5) (Wu et al., 2013, Fig. 7). Amplitude modulation (AM) analysis also shows 2.6 myr and 1.05 myr periods in eccentricity bands, and 2.9 myr, 1.95 myr, 1.44 myr and 0.99 myr periods in obliquity bands in the SB (Wu et al., 2013, Figs. 9, 10). In the WIS Niobrara Formation the ~1.7 myr period was interpreted as precession modulation (Fig. 7) (Locklair and Sageman, 2008).

Long-term base-level cycles are recorded in both the SB and the WIS. In each basin the cycle sets change up-section and become sand-dominated as basinal tectonics changed. However base-level cycles in the two basins differ in timing, durations and facies sets. In the SB an upper Campanian condensed section or unconformity separates two second-order cycles, each of which average 13.5 myr in duration. In the WIS three second-order cycles are separated by major unconformities at uppermost Turonian and upper Campanian strata and average 10.5 myr in duration.

The second-order sequences in the SB are composed of fining-up third-order sequences of fluvial, deltaic, and lacustrine facies; maximum flooding is represented either by dark gray, organic-rich shale or lacustrine shale and sandstone. In the WIS the long-term cycles are composed of marine facies successions of dark gray shale, pelagic carbonates and shale that grade shoreward into sandstone.

5. Late Cretaceous paleoclimates of the two basins

Diverse methods and data make possible the comparison of different environmental conditions in the SB and WIS basins. The Late Cretaceous paleoclimate frameworks of both basins were constrained by global current modeling and paleoclimate reconstruction (Pucéat et al., 2005; Haggart et al., 2006; Boucot et al., 2009), global vegetation simulations (Otto-Bliesner and Upchurch, 1997; Upchurch et al., 1998; Donnadieu et al., 2009; Fricke et al., 2010), and the climate proxy $\delta^{18}O$. The $\delta^{18}O$ record of lake water reflects a balance of the interplay between climate and drainage basin evolution, although it may have been compromised by some diagenetic effects (Chamberlain et al., 2013). The ratio of $^{86}Sr/^{87}Sr$, spore/pollen, paleoecology, and climatically sensitive deposit data of the Songliao Basin, and the Far East marine $\delta^{18}O$ record were also used to better constrain interpretations. Following the classification of modern world climates zones by Köppen, the Cretaceous paleoclimate zones are subdivided into the tropical zone, the arid zone, the warm temperate zone, the cool temperate zone, the cold zone, and the paratropical (subtropical) zone (Boucot et al., 2009).

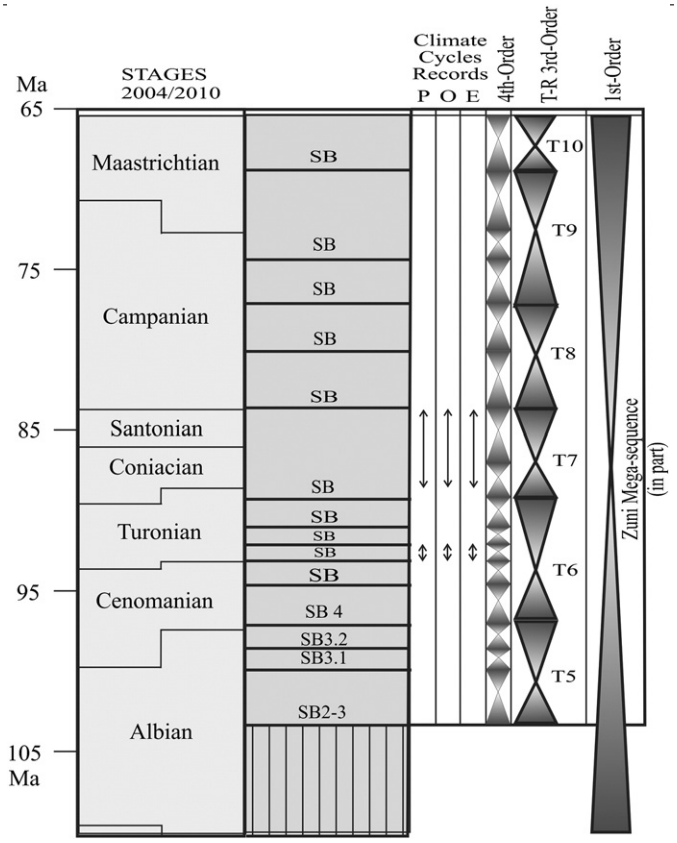

Fig. 6. Depositional sequences of the Western Interior Basin center based on Kauffman (1977, 1984). Albian–Cenomanian sequences defined by Oboh-Ikuenobe et al. (2008); late Cenomanian–Coniacian sequence defined by Gardner and Cross (1994), Leithold (1994), and Merewether et al. (2007). Stratigraphic intervals of higher-level climatically driven cycles shown by arrows (see Fig. 7). This section is the Upper Cretaceous part of the Middle Jurassic through Cretaceous Zuni Mega-sequence (Sloss, 1963). Numerical ages of stage boundaries calibrated by two different methods; Ogg et al. (2004) interpolated ages between radiometric dates; Scott et al. (2004) and Scott (2009) used graphic correlation to integrate global sections with dates. SB stands for sequence boundary. P, O, and E stand for precision, obliquity, and eccentricity, respectively.

5.1. Paleoclimate of Songliao Basin

The Songliao Basin offers a unique opportunity to understand the Cretaceous paleoclimate of terrestrial settings because it contains a nearly complete record of Late Cretaceous lacustrine sedimentation (Chen, 1987; Chen and Chang, 1994). Here we only discuss the strata recovered from SKI, including a portion of the Quantou Formation (late Albian–middle Turonian), the Qingshankou Formation (middle Turonian–late Coniacian), the Yaojia Formation (late Coniacian–late Santonian), the Nenjiang Formation (late Santonian–early Campanian), the Sifangtai Formation (early Campanian–late Campanian), and the

Fig. 5. Cyclostratigraphic interpretation and sedimentary accumulation rates of the SKI south core in Songliao Basin. Magnetostratigraphy results and SIMS U-Pb zircon ages are from He et al. (2012). Paleoenvironmental data are from Cheng et al. (2009), Gao et al. (2009), P.J. Wang et al. (2009) and G.D. Wang et al. (2009). The numbers at the Member column are the ATS ages in "Ma" for the strata boundaries. The "e" (blue) and "E" (red) represent 100 kyr short and 405 kyr long eccentricity cycles, respectively. Filter passband for 405 kyr eccentricity cycles: K2n1 + 2—0.0156 ± 0.0027 cycles/m, K2y—0.021 ± 0.004 cycles/m, K2qn—0.0261 ± 0.005 cycles/m, and K2q3 + 4—0.0127 ± 0.0036 cycles/m. Filter passband for 100 kyr eccentricity cycles: K2n1 + 2—0.0625 ± 0.0189 cycles/m, K2y—0.0859 ± 0.025 cycles/m, K2qn—0.113 ± 0.025 cycles/m, and K2q3 + 4—0.0508 ± 0.0116 cycles/m. Modified from Wu et al. (2013).

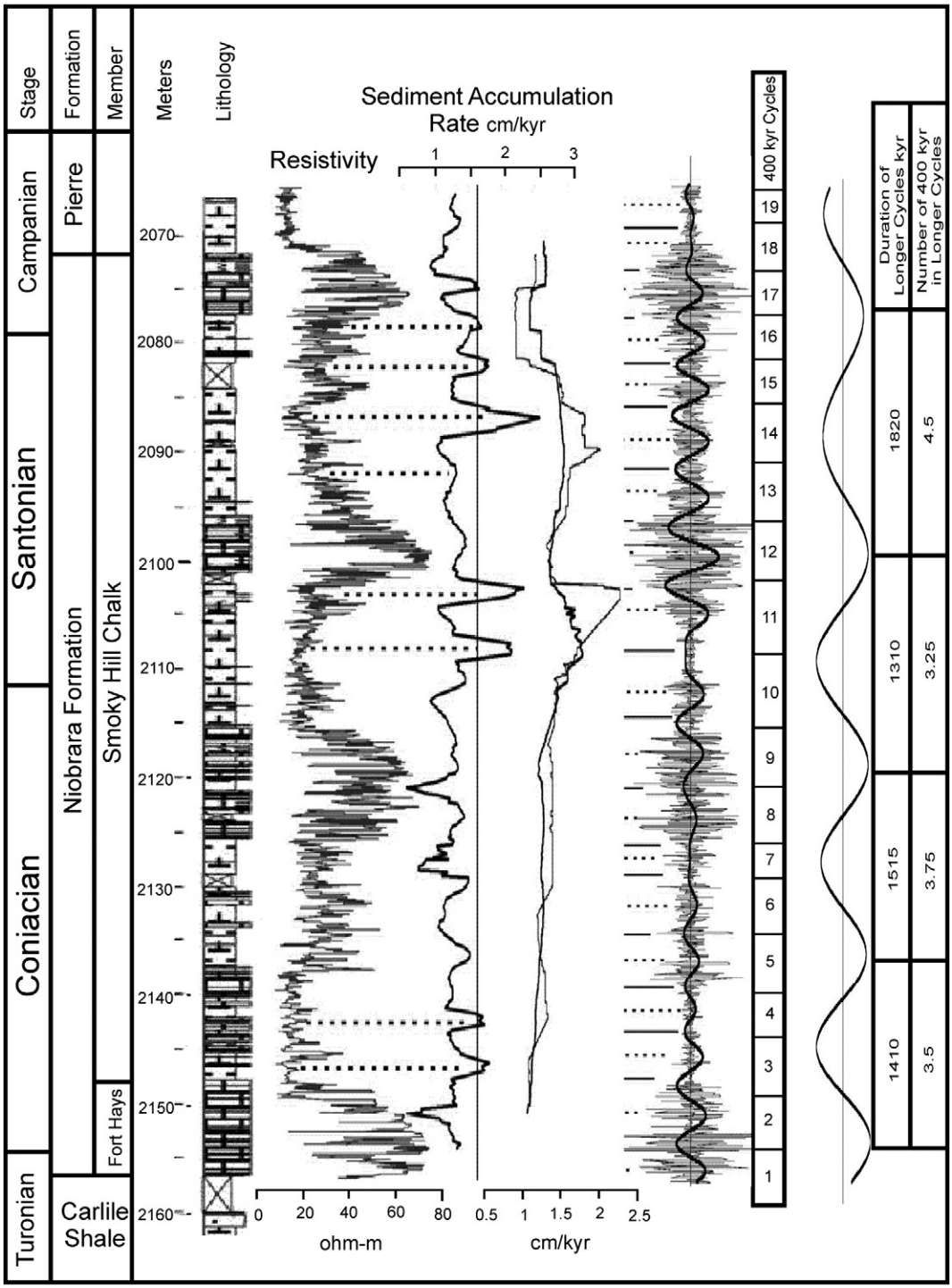

Fig. 7. Cyclostratigraphy and sediment accumulation rate of the Niobrara Formation in a north-central Colorado well (Locklair and Sageman, 2008, Figs. 4, 5, 7). Lithology indicated by resistivity curve. Eight dashed lines correlate intervals of higher rates with more argillic units. Sediment accumulation rate (left curve) was calculated by bandpass frequency analysis of short eccentricity (100 kyr). Two right-hand curves were calculated by evolutive analysis and are time-averaged; the bold, high frequency curve tracks obliquity and the narrow, long frequency curve tracks eccentricity (Locklair and Sageman, 2008, Fig. 7).

Mingshui Formation (late Campanian–Cretaceous/Paleogene) (see Section 3 of this paper).

The climate history of the Songliao Basin is based on pollen and spore ratios (Fig. 8) (Gao et al., 1999) using more than 20,000 samples from more than 500 cores. The Cretaceous vegetation landscape of the basin fluctuated between a conifer forest and an herbaceous-broad-leaved forest (Fig. 8). Climates of the Songliao Basin are compared with the marine oxygen isotopic data of Far East (Zakharov et al., 1999; Fig. 8); paleotemperature zones are defined by the spore/pollen spectra in the SB, and the oxygen isotopic trends of Songliao Basin (Chamberlain et al., 2013).

The oxygen isotope record of the Qingshankou Formation through the middle part of the Mingshui Formation is based on data from ostracods collected in the SKI core (Fig. 8) (Chamberlain et al., 2013). These oxygen isotope data record five distinct shifts. The trend of the oxygen isotopic data is similar to the global marine record (Friedrich et al., 2012). Chamberlain et al. (2013) argued that diagenesis did not play a major role in the isotopic results and interpreted the isotopic record of

the Songliao basin to broadly reflect the global evolution of climate system during the Late Cretaceous. Trend 1 is a strong negative oxygen isotope shift in the Turonian part of the Qingshankou Formation (Fig. 8). This negative shift represents warming and was attributed to global changes in the hydrologic/carbon cycle (Chamberlain et al., 2013). The paleoenvironment is dominantly a subtropical, semi-humid, conifer and broad-leaved, evergreen forest that corresponds with warming to 15°–17° in the Far East (Fig. 8). Trend 2 is composed of three fluctuations of the oxygen isotopes representing cooling following the negative shift of trend 1. Oxygen isotopes in the Coniacian part of the upper Qingshankou increase to −10‰, then decrease slightly in the Santonian Yaojia Formation. The oxygen isotope values increase again to −6–8‰ in the first through fourth members of the upper Santonian to lower Campanian Nenjiang Formation. The paleoenvironment is a subtropical, humid to sub-humid, broad-leaved and conifer forest. Marine foraminifera are present in the Qingshankou and the 1st and 2nd members of the Nenjiang Formation, indicating marine water incursion into the Songliao Basin (Xi et al., 2011b). We assume that the positive shifts resulted at least partly from marine incursions and correlate with cooling to 10° in the Far East with a brief warm spike in the early Santonian (Fig. 8). Trend 3 has generally decreasing isotope values from the middle Campanian fifth member of the Nenjiang to the middle-upper Campanian Sifangtai Formation. The paleoenvironment is a subtropical, semi-arid, herbaceous and broad-leaved, deciduous forest. This warming period corresponds with Far East warming in the Campanian (Fig. 8). Trend 4 is an abrupt increase in $\delta^{18}O$ values to ~5‰ at the boundary between the Sifangtai and Mingshui formations and continuing into the Maastrichtian lower Mingshui Formation and corresponds with a temperature decline from about 20° to 10°. The paleoenvironment is a subtropical, semi-humid, conifer and herbaceous forest. Trend 5 has positive $\delta^{18}O$ values through the middle Maastrichtian middle Mingshui with a short spike at the top of the data. The paleoenvironment is a temperate, semi-humid, mixed conifer and herbaceous forest and corresponds with brief Maastrichtian cooling–warming–cooling fluctuations (Fig. 8).

In the absence of Cenomanian–lower Turonian oxygen isotope data, SB climates are based on pollen/spore data. The Quantou Formation was deposited during a semi-humid subtropical environment and the latest Maastrichtian uppermost Mingshui Formation during a semi-humid warm temperate environment.

In conclusion, the oxygen isotope data and spore/pollen data from the Songliao Basin broadly reflect the global evolution of climate system during the Late Cretaceous. The general trends of the spore/pollen data and oxygen isotope data from the Songliao Basin and Far East are similar. The global paleovegetation simulations (Otto-Bliesner and Upchurch, 1997; Upchurch et al., 1998; Sewall et al., 2007; Donnadieu et al., 2009; Fricke et al., 2010) are consistent. The major vegetation type of the Late Cretaceous Songliao Basin was a broad-leaved evergreen forest, reflecting temperate and humid climate conditions; the southern part was adjacent to arid areas, and had a slightly arid climate during some Cretaceous stages. The temperature was above 0 °C throughout the year, and rainfall was relatively abundant. Based on all the information above, we conclude that the Songliao Basin was mainly in a humid to semihumid warm temperate-subtropical climate in the Late Cretaceous. This conclusion is also supported by the global paleoclimate reconstruction of climatically sensitive deposits (Boucot et al., 2009). East Asia, including the Songliao Basin, was in the warm temperate zone during most of the Late Cretaceous (Fig. 1a), and did not experience large climatic changes. In a greenhouse world without ice caps, ancient ocean currents became the primary controls of continental climate changes (DeConto et al., 1999; Hay, 2008, 2011). The Songliao Basin was influenced by northward flowing warm currents from the Pacific equatorial regions and cold currents flowing southward from the Arctic (Pucéat et al., 2005; Haggart et al., 2006). These currents approximately correspond to the modern Kuroshio and Oyashio currents, because Pacific oceanic circulation patterns offshore of the Songliao Basin were broadly similar to those of today, keeping a relatively stable state (Gordon, 1973; Klinger et al., 1984). Because these two ancient ocean currents mixed east of the Songliao Basin (Fig. 1c), they certainly affected the climate, depositional systems, and biotic assemblages.

5.2. Paleoclimate of the Western Interior Seaway

The WIS was a shallow, elongate north-to-south basin. Runoff from the eastern margin flowed northerly and western nearshore currents flowed southerly. Warm saline Tethyan waters were drawn in from the south and cool lower salinity waters entered from the Arctic Ocean. In the WIS, modeled salinity ranged from 37 ppm to 33 ppm in a south to north gradient (Slingerland et al., 1996). The influence of

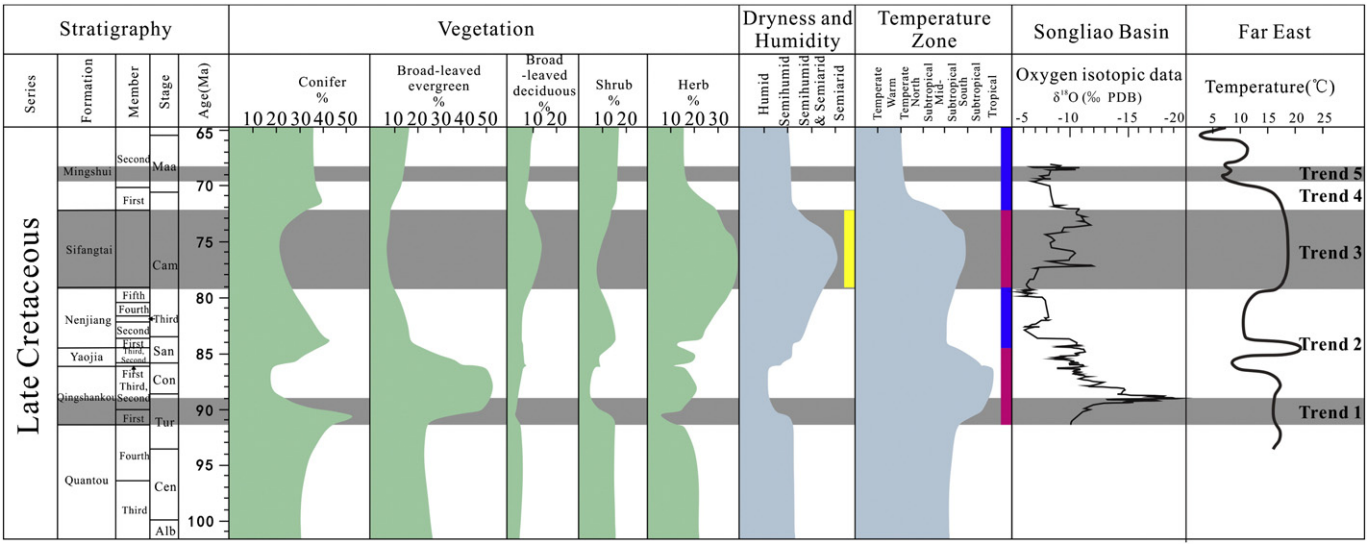

Fig. 8. Cretaceous paleoclimate evolution of the Songliao Basin. Spore/pollen relative abundances, paleotemperature zones and paleohumidity are from Gao et al. (1999). Those of the Far East are from Zakharov et al. (1999). The oxygen isotope data are from Chamberlain et al. (2013). The classification of temperature zones is based on the species of spore/pollen spectra that define the tropical, tropical–subtropical, subtropical, tropical–temperate, and temperate. The dryness and humidity are based on species of parent plants of spore/pollen fossils subdivided into xerophyte, mesophyte, hygrophyte, helophyte, and hydrophyte, which correspond to arid, semiarid, semihumid & semiarid, semihumid, and humid, respectively. The red bars indicate warming stages; the blue bars indicate cooling stages, and the yellow bars indicate semiarid stage.

northern freshwater probably reached as far south as Kansas, and with relatively little inflow of surface waters from the Tethys Ocean to the Western Interior Seaway, supports a model of a northern gyre, possibly reversing seasonally (Coulson et al., 2011). In the Western Interior, the Maastrichtian Pierre Shale, Fox Hills and Hell Creek Formations record offshore to freshwater depositional environments (Cochran et al., 2003). The $^{87}Sr/^{86}Sr$ ratios suggest that paleosalinity decreased from about 35‰ in the open marine condition to a minimum of 20‰ in the brackish facies.

Atmospheric temperatures in the WIS are estimated by plant megafossils, spores and pollen. At all latitudes the annual climate was seasonal, and at northern latitudes the plants adapted to winter dormancy and possibly freezing temperatures (Upchurch and Wolfe, 1993; Spicer and Herman, 2010). The long-term temperature trend in the WIS at about 30°N paleolatitude varied up to 6 °C, from 21 °C in the Albian to 25 °C in the Coniacian–Santonian followed by Campanian to early Maastrichtian cooling to about 22 °C, and as warm as 27 °C in the latest Maastrichtian (Upchurch and Wolfe, 1993; Spicer and Herman, 2010). Marine oxygen isotope data for the Albian and Upper Cretaceous from the Western Interior Seaway (Fig. 9; Pratt et al., 1993; Burns and Bralower, 1998; Cochran et al., 2003; Keller et al., 2004; He et al., 2005; Caron et al., 2006; Zakharov et al., 2006) are evidence of a Late Cretaceous declining paleotemperature trend. Diagenetic effects seem minimal because ammonoids, planktic foraminifera, and nannoplankton are moderately to well preserved (Burns and Bralower, 1998; Keller et al., 2004; Caron et al., 2006). The highly negative $\delta^{18}O$ in the records was affected by fresh-water runoff and mixing with northern Arctic waters (Burns and Bralower, 1998; Keller et al., 2004). Oxygen-isotope compositions of the seawater in the Cenomanian WIS were low, near −8‰ (Whittaker et al., 1987; Cadrin et al., 1996). Then the $\delta^{18}O$ values increased with transgression and northward spread of Tethyan water, reaching −2‰ in the early Turonian (Cadrin et al., 1996). After this increase, the mean $\delta^{18}O$ value of seawater decreased to ~−4‰ from the Coniacian to the late Santonian (Coulson et al., 2011). The Early Campanian WIS had average values near −1‰, similar to those of the modern ocean (Whittaker et al., 1987; Cochran et al., 2003; Zakharov et al., 2006).

These WIS data record oxygen isotope shifts in three stratigraphic intervals: the Cenomanian–Turonian transition, the uppermost Turonian–Santonian, and the Upper Campanian–Maastrichtian. A mixed paleotemperature/salinity fluctuation spanned the 2 myr Cenomanian–Turonian transition, where the $\delta^{18}O$ values change from ~−12‰ to −5‰ up to the boundary and then back to about −10‰ in basal Turonian. Above the boundary in the lower Turonian, the oxygen isotopes values are relatively stable at ~6‰ (Fig. 9; Keller et al., 2004; Caron et al., 2006). Small positive $\delta^{18}O$ shifts across this boundary are also recorded in ODP site 869 in the Pacific Ocean (Jenkyns et al., 1995) and in Austria (Wagreich et al., 2008). The minimum $\delta^{18}O$ value −12‰converts to a temperature of 26 °C with a sea water oxygen isotope value of −8‰ (Keller et al., 2004). In the uppermost Turonian–Santonian, the oxygen isotopes are between −5‰ to −6‰ and gradually increase upward (Fig. 9; He et al., 2005; Pratt et al., 1993). Oxygen isotopes in biophosphate from coeval marine turtle and fish fossils from the east central seaway yield a temperature of 27.1–27.8 °C during the this period (87–82 Myr) (Coulson et al., 2011). Late Campanian–Maastrichtian paleotemperature decreased, which is indicated by more positive isotope data than the previous periods (Fig. 9; Cochran et al., 2003; Zakharov et al., 2006). This change is similar to continental and marine records (Pucéat et al., 2003; Amiot et al., 2004). Sea surface paleotemperatures were calculated from 19.2–23.7 °C (late Campanian), then to 20.1–25.3 °C (early Maastritchtian) and to 13.2–24.9 °C (late Maastrichtian) (Zakharov et al., 2006). The carbonate clumped isotope thermometer (Δ47) of macrofossils indicate temperatures ranging from 24.2 ± 0.4 °C (~73.5 Ma) to 16.4 ± 3.5 °C (67 Ma) for a Late Cretaceous off shore Western Interior Seaway environment (Dennis et al., 2013).

The modeling studies of the WIS in the Late Cretaceous are consistent with the information above. Bush and Philander (1997) predicted an annual mean near-surface temperature of 15–20 °C, and a ±15 °C seasonal cycle. Otto-Bliesner et al. (2002) predicted a mean annual atmospheric temperature of between 20 and 25 °C, and an annual mean sea surface temperature (SST) of 18–24 °C. Climate-sensitive deposits (coals, calcrete, and kaolinite) in the Western Interior Seaway indicate a humid, warm climate in the Western Interior seaway in the Late

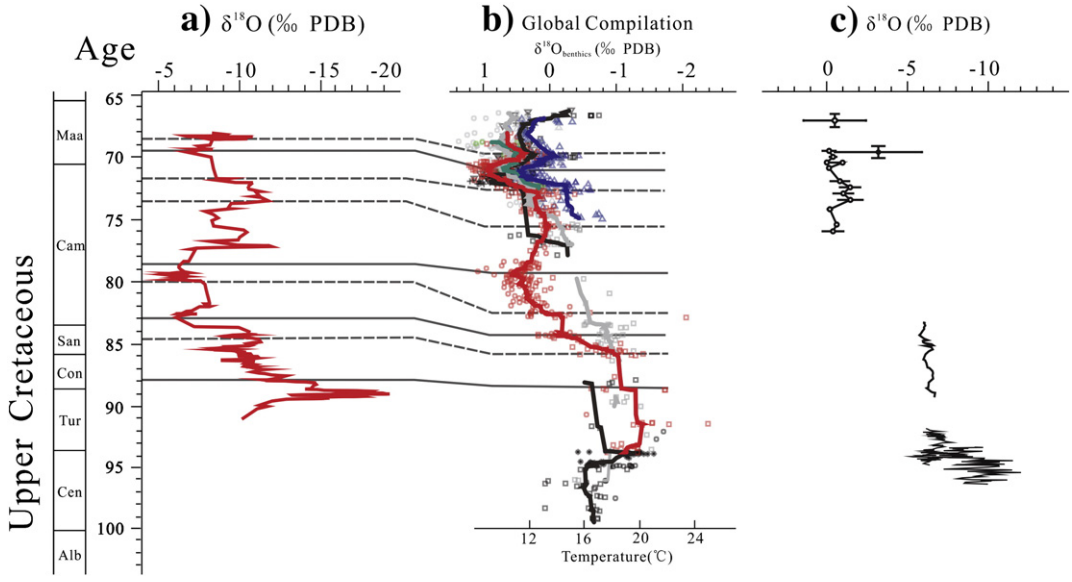

Fig. 9. Upper Cretaceous (Cenomanian–Maastrichtian) changes in (a) stable oxygen isotope of the Songliao Basin (Chamberlain et al., 2013); (b) stable oxygen compilation of benthic foraminifera of Cretaceous oceans (Friedrich et al., 2012). Thick lines represent trends through data of individual ocean basins (running mean with a 5-point window for the Indian Ocean and 15-point window for all other data). Black = North Atlantic, gray = southern high latitudes, red = Pacific, blue = subtropical South Atlantic, green = Indian Ocean. Dark gray (dashed) lines are guides to comparison of paleotemperatures between each the Songliao Basin and Cretaceous oceans; (c) stable oxygen isotope of the WIS (Western Interior Seaway), data are from Pratt et al. (1993), Cochran et al. (2003), Keller et al. (2004), He et al. (2005), Caron et al. (2006), and Zakharov et al. (2006).

Cretaceous, and the paleoclimate did not change greatly (Boucot et al., 2009; Fig. 1b).

5.3. Comparison

The Late Cretaceous climate (Hay, 2009, 2011) gradually cooled from the warmest Albian–Cenomanian time to the end of the Maastrichtian with several intervening warm periods. The Songliao Basin climate was humid to semihumid warm temperate–subtropical and the central part of the Western Interior Seaway was in the humid warm temperate zone. During the Late Cretaceous both basins were at middle latitudes in the Northern Hemisphere, and experienced only moderate climatic changes. This comparison is supported by global paleoclimate reconstruction of climatically sensitive deposits, flora and oxygen isotopes. The average temperature of the warm temperate climate in the SB was above 10 °C in the warmest months, and in the coldest months the average was between −3 °C and 18 °C. Thus, the average Cretaceous temperature in SB was at least 5 °C degrees warmer than the present mean annual temperature of 4.9 °C (Zheng et al., 2010). The Cretaceous warm temperature belt extended as far north as about 50°N latitude, and the present mid-latitude warm temperate zones became subtropical in the late Cretaceous. Cretaceous terrestrial records model this trend in eastern China. Cretaceous deserts and continental red beds are mainly distributed in southern China, and a more humid and warmer climate with coal and peat deposits prevailed in North China (Xiang et al., 2009).

Based on the comparison of the SB and WIS, climatic fluctuations of terrestrial systems were more intense and abrupt than in marine systems. Oxygen isotope data of the Songliao Basin are between −5‰ and −20‰, and the shifts were frequent and sharp. The WIS records were affected by fresh-water runoff and mixing with northern Arctic waters. The shifts were between the continental and marine records, ranging from −10‰ to 0‰ and shifts were more gradual (Pratt et al., 1993; Cochran et al., 2003; Keller et al., 2004; He et al., 2005; Caron et al., 2006; Zakharov et al., 2006). This difference is not surprising, because the $\delta^{18}O$ of the Songliao Basin should reflect changes in relative humidity, temperature, and evaporation in the drainage basin.

The isotopic record of the Songliao basin broadly reflects the global climate system evolution during the Late Cretaceous, except trends 1 and 5 (Fig. 8), which were very different from marine records and are attributed to be the result of global changes in the hydrologic/carbon cycle and local drainage reorganization within the basin (Chamberlain et al., 2013). The $\delta^{18}O$ trends are comparable between the Songliao Basin and Cretaceous oceans (data of WIS are too scarce to discuss), however all the shifts in the Songliao Basin generally lag behind the changes in the Cretaceous oceans (Fig. 9). Most of the time the lags are some 1.5–2 myr, except two of these are less than 1 myr. Although the reasons are unknown, we assume that the continental climate was influenced and partly controlled by the ocean climate changes, and that continental climate responded more slowly than the oceans.

The latitudinal climate differences of the Cretaceous greenhouse world were smaller than during the icehouse world. Paleotemperature data inferred that the global ocean latitudinal gradient (middle latitude) was 0.26 °C/1° latitude (Hu et al., 2012) in the Late Cretaceous. Maastrichtian atmospheric temperatures estimated by leaf physiognomy were 16–25 °C at a paleolatitude of about 38°N in New Mexico and ranged from 6.3 ± 2.2 to −2.0 ± 3.9 °C at 82°N latitude (Scherer et al., 2002; Spicer and Herman, 2010). These data suggest a North American terrestrial latitudinal gradient of about 0.36 °C/1° latitude in the Maastrichtian. This value is similar to the 0.3 °C per degree of latitude from Wolfe et al. (1987) and 0.4 °C per degree of latitude from Dworkin et al. (2005). We infer that the same gradient (0.36 °C/1° latitude) existed in the Late Cretaceous Songliao Basin. The latitudinal gradient of modern middle latitudes is about 0.5 °C/1° latitude and nearly 0.7 °C/1° latitude for ocean and continent (Hay, 2011; Hu et al., 2012). It seems that Late Cretaceous paleoclimate of the middle latitudes in the Northern Hemisphere was more "moderate" than the present.

6. Timing and processes of organic carbon deposition

Organic carbon accumulation in sedimentary basins is important not only for hydrocarbon source rocks, but also for understanding the global carbon cycles in deep time. The Cretaceous Songliao Basin and Western Interior Seaway are well known terrestrial and marine oil- and gas-bearing basins. Because the SB is located at the same latitude as the middle part of the WIS, they provide a unique opportunity to understand climatic effects on mass accumulation of organic carbon. Organic carbon accumulation in these basins spanned the time of Cretaceous oceanic anoxic events 2 and 3 (Huang et al., 2013; Wu et al., 2013). Comparison of organic carbon burial in marine and terrestrial realms may contribute to understanding the global carbon cycle (Fig. 10).

6.1. Songliao Lacustrine Basin

The principal source rocks for the Daqing Oilfield in the Cretaceous Songliao Basin (SB) are member 1 of the Qingshankou Formation and members 1 and 2 of the Nenjiang Formation (Yang et al., 1985; Hou et al., 2000). These two source rock units are distributed in an oval area in the multiple structural depressions of the SB (Fig. 11) (Yang et al., 1985; Wang et al., 2006). Corresponding to the spatial lithofacies change in the source rocks, the organic-carbon content generally increases basinwards. For example in most of the central depression area, the organic carbon content of member 1 of the Qingshankou is higher than 2.0%, and can be as high as 20% in the oil shales; at the basin margins it is less than 2.0%.

SKI south well recovered core from members 3–4 of the Quantou Formation to the top of member 1 of the Nenjiang Formation (Fig. 11). The TOC content of the members of these formations vary greatly and few are source rock quality (Table 2; Feng et al., 2009). Lake level became shallower during deposition of members 2 and 3 of the Qingshankou Formation, which did favor the preservation of organic matter (Feng et al., 2009). The deposition of the Yaojia and Nenjiang Formations indicates another shallow to deep cycle of basin evolution after the deposition of the Quantou and Qingshankou Formations. Previously, the brown and red siliciclastics of the Yaojia were considered to have a very low TOC. The relatively higher values in this core indicate that semi-hypolimnal facies were developed locally and that member 1 of the Yaojia Formation formed a source rock. But TOC content of members 2 and 3 of the Yaojia is very low. However the TOC content and relative indices increase in members 1 and 2 of the Nenjiang Formation.

The Upper Cretaceous stratigraphic distribution of TOC in the SKI core is cyclical and up to nine cycles can be discerned in the lithologic column. The TOC is high in the lower part and decreases in the upper parts of each cycle. Member 1 of the Qingshankou Formation is divided into two cycles. The TOC at the base of member 1 is as high as 8.35% but decreases to 0.5% in the upper part. In the second cycle the peak TOC is 9% in the lower part. The variation of organic content for different cycles was controlled both by the subsidence of the basin and climate. In each cycle, the sedimentation rates, productivity and redox condition of the bottom waters were important for deposition and preservation of organic matter (Feng et al., 2009).

The durations of member 1 of the Qingshankou Formation, and members 1 and 2 of the Nenjiang Formation are about 0.94 myr (from 91.37 to 90.44 Ma) and 1.38 myr (from 83.88 Ma–81.5 Ma), respectively (Deng et al., 2013; Wu et al., 2013). Sequence stratigraphic analysis indicates that at these two times the paleo-Songliao lake was greatly expanded (Wang and Liu, 2001). The SB was more than 100 m deep and wide enough to minimize detrital clastic influx into the depositional center of the basin (Feng et al., 2010; Wang et al., 2013), which promoted organic carbon accumulation and burial.

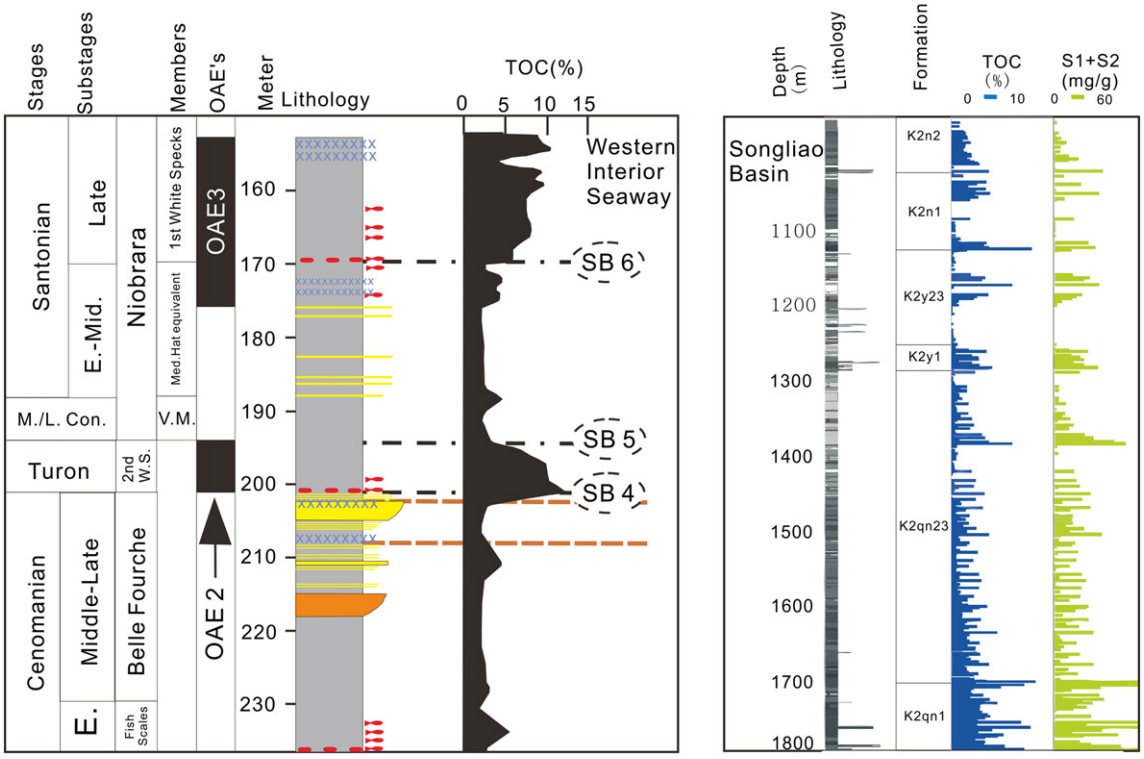

Fig. 10. TOC correlation of Niobrara Formation of Western Interior Seaway (Schröder-Adams et al., 2012, Fig. 2) and Qingshankou to Nenjiang formations (middle Turonian to earliest Campanian) of Songliao Basin (see Figs. 4 and 5 for designation of stratigraphic units). Second White Specks lithostratigraphic unit indicated by 2nd w.s. V.M. indicates Verger Member of Niobrara Formation. Regional sequence boundaries are from the SB.

The organic carbon burial rate (0.80 g TOC/cm^{-2}/kyr) in member 1 of the Qingshankou Formation was calculated based on the average organic carbon content (3.5%), sedimentation rate (9.8 cm/kyr) and density of the black shale (2.5 g/cm^3). The average rate is more than twenty times higher than the rate of the OAE 2 interval (approximately 0.03 g TOC/cm^{-2}/kyr) in the Western Interior Seaway (Meyers, 2007). If this number represents the organic carbon burial rate of member 1 of the Qingshankou Formation in the Songliao Basin with a total depositional area of 7×10^4 km^2 (Ye et al., 2002), the annual organic carbon burial rate would have been 0.616 Tg/yr. In members 1 and 2 of the Nenjiang Formation the average rate of organic carbon burial is based on assuming 3.5% for total organic carbon, 21.7 cm/kyr for sedimentation rate, and 2.5 g/cm^3 for density. For members 1 and 2 of the Nenjiang Formation, the organic carbon burial rate is 1.89 Tg/yr with a total depositional area of 10×10^4 km^2 (Ye et al., 2002). However as this is just one well from the deep lake facies with higher organic carbon content, it cannot represent the entire basin. The average TOC levels of shallower facies are always higher than 1% and if we take this as the lower limit, then the annual organic carbon burial rate would be 0.175 and 0.543 Tg/a for member 1 of the Qingshankou Formation, and members 1 and 2 of the Nenjiang Formation, respectively.

The organic matter of the source rocks in the Songliao Basin originated from lacustrine algae with little terrestrial input. Organic matter types I and II are dominant in both formations and type III is minor in the Qingshankou Formation. This is consistent with petrographic examination of thin sections. Black shale facies and dark mudstone are composed of algal-rich laminae (Fig. 12). This is demonstrated by rock pyrolysis data of H/C–O/C, HI–OI and HI–Tmax (Gao et al., 1994; Bechtel et al., 2012). TOC correlates with the hydrogen index (HI) as expected for source rocks. The HI is less than 200 mg/gTOC where the organic carbon is less than 1%, but where TOC is higher than 3%, the HI increases dramatically up to 700 mg HC/g TOC (Gao et al., 1994). Biomarker studies also support this conclusion (Gao et al., 1994).

Numerous studies have shown that the Songliao Basin was mainly a fresh-water lake during most of its history. However the lake became saline during the deposition of oil-prone shale in member 1 of the Qingshankou Formation and members 1 and 2 of the Nenjiang Formation (Hou et al., 2000; Bechtel et al., 2012). Evidence of lake salinization during source rock deposition is the abundant ferruginous dolomite laminae intercalated in shales of member 1 of the Qingshankou and members 1 and 2 of the Nenjiang both in outcrops and cores (Wang and Liu, 2001; Gao et al., 2010). In the SKI core 62 dolomite layers are found in member 1 of the Nenjiang Formation, and dolomitic black shale is developed in member 1 of the Qingshankou, but the origin of dolomite in Songliao Basin is still controversial (Warren, 2000). Marine calcareous nannofossils (Huang and Huang, 1998) and planktic foraminifera (Xi et al., 2011b) also indicate saline water conditions for the deposition of source rock in the paleo-Songliao Lake.

Additional paleontological evidences of a marine incursion are dinoflagellate steranes in oil shale (Hou et al., 2000) and shark teeth and benthic foraminifera in member 1 of the Qingshankou and members 1 and 2 of the Nenjiang Formations (Zhang et al., 1977; Xi et al., 2011b). The marine influence of the Songliao paleo-lake is supported by sulfur geochemistry because fresh and marine waters have different levels of sulfate. Pyrite sulfur isotope ratios average 18.5‰ (ranging from 14.4 to ~24.1‰), which is very close to that of the coeval marine value of ~19‰ (Paytan, 2004; Huang et al., 2013).

Marine incursion from the western Pacific, rather than climatic factors, such as evaporation was the most likely reason for the salinization of the Songliao Lake during source rock deposition (Hou et al., 2000). Saline marine incursion would stimulate organic carbon deposition in the basin. In saline waters, especially with the introduction of sulfate, pyrite forms in either the anoxic water column or pore-water of sediments as the result of reduction of sulfate and ferric oxides, which then increases the release of phosphate from sediments (Van Cappellen and Ingall, 1994; Gächter and Müller, 2003). Phosphorus enhances surface water

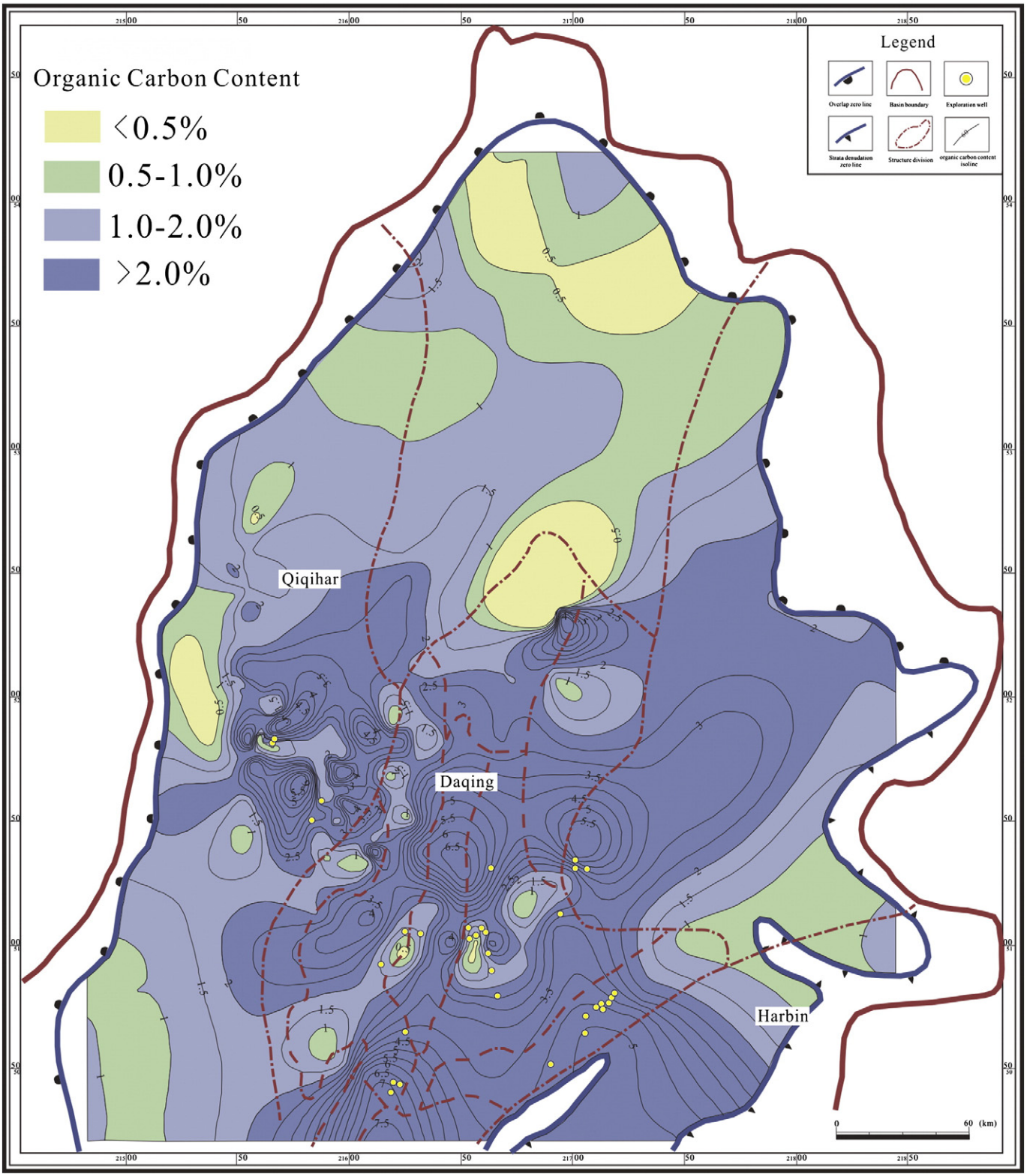

Fig. 11. Organic carbon percent in members 1 and 2 of the Nenjiang Formation of the Songliao Basin. The principle source rocks are distributed in an oval area including several structural depressions of the SB (Yang et al., 1985; Wang et al., 2006). Corresponding to the spatial lithofacies change in the source rocks, the organic-carbon content generally increases basinwards.

productivity and growth of aquatic biota (Caraco et al., 1993; Tyrrell, 1999; Meyers, 2007). A positive feedback loop develops between productivity and limnic anoxia, i.e., the more anoxic the lake becomes, the higher aquatic production (Van Cappellen and Ingall, 1994). Such feedback will dramatically increase the burial of organic carbon in the lake sediments. Evidence of this process is that the molecular ratio of organic carbon to phosphorus in the oil-shale is 9 to 17 times greater than normal (Huang et al., 2013). The most reasonable interpretation for this phenomenon is that more phosphorus was preferentially generated relative to the organic carbon and returned to the water column when the feedback loop was running (Van Cappellen and Ingall, 1994; Meyers, 2007).

Table 2
The TOC, S1 + S2[a], Chloroform bitumen A for each stratigraphic unit of the Songliao Basin.[b]

Stratigraphic unit	TOC (%)	S1 + S2 (mg/g)	Chloroform bitumen A (%)
Quantou Formation	Mean of 0.2 Range from 0.12 ~ 0.4	0.14	
Member 1 of the Qingshankou Formation	Mean of 3.21 Range from 0.125 ~ 9.08	5	0.49
Members 2 and 3 of the Qingshankou Formation	Mean of 1.35	9.88	0.31
Member 1 of the Yaojia Formation	Mean of 1.45	12.51	0.56
Members 2 and 3 of the Yaojia Formation	Very low	Very low	Very low
Members 1 and 2 of the Nenjiang Formation	Mean of 1.5	5.5	0.18

[a] S1 and S2 are the free and residential hydrocarbon of the source rock during the pyrolysis, respectively. The sum of S1 and S2 stands for the source rock potential.
[b] Modified from Feng et al. (2009).

6.2. Western Interior Marine Basin

In the North American Western Interior Basin (WIS) two Late Cretaceous oceanic anoxic events (OAEs) are recorded, one in the Cenomanian–Turonian Greenhorn Formation (OAE 2) (Pratt, 1984; Elder, 1985) and the other in the Coniacian–Santonian Niobrara Formation (OAE 3) (Fig. 10) (Leckie et al., 2008). OAEs were globally widespread episodes of organic-carbon (OC) burial in marine sequences (e.g., Schlanger and Jenkyns, 1976; Arthur and Schlanger, 1979; Jenkyns, 1980; Arthur et al., 1987; Schlanger et al., 1987; Arthur et al., 1990) that represent periods of widespread oxygen deficiency in oceanic mid- and deep-water masses (Fig. 10). The widespread occurrence of OAEs in time and space during the middle Cretaceous implies fundamental changes in oceanic circulation and/or in the rate and mode of delivery of organic matter to the deep sea. The origin of the OAEs is not known for certain, but available data suggest that such events resulted from some combination of higher phytoplankton productivity and enhanced preservation under oxygen-depleted deep-water masses.

The Greenhorn and Niobrara Formations are the only two marine carbonate units in a thick sequence of detrital mud rocks that represent periods of maximum transgression into the Western Interior Seaway (WIS) when the shoreline reached as far as western Utah. At these times, the seaway was deep enough and wide enough to minimize detrital clastic influx into the depositional center of the basin in western Kansas and eastern Colorado where pelagic/hemipelagic limestones are interbedded with marlstone and calcareous shale. These carbonate-rich units are also the most OC-rich, containing up to 8% OC in the laminated to partially bioturbated marlstone beds (Pratt et al., 1993; Dean and Arthur, 1998b). The thick sequences of dark gray, non-calcareous mud rocks that dominate the Cretaceous stratigraphic section in the WIS generally contain <1% OC, except in the Sharon Springs Member of the Campanian Pierre Shale where OC values as high as 11% have been reported (Parrish and Gautier, 1993). The Albian–Cenomanian Mowry Shale, is an important hydrocarbon source rock in the Northern Rocky Mountain area, but contains an average of only about 2.5% OC (Burtner and Warner, 1984; Finn, 2010).

The Niobrara Formation is an important source and reservoir for biogenic and thermogenic petroleum in eastern Colorado. The Niobrara and the underlying Codell Sandstone Member of the Carlile Shale contribute 67% of the total oil and 34% of the total gas production in the Wattenberg field in the west-central part of the Denver Basin (Higley and Cox, 2007).

The Albian to Santonian Cretaceous WIS section (about 305 m (1000 ft) and 20 Myr) was cored in the Amoco No. 1 Bounds well in western Kansas (Fig. 13) (Dean et al., 1995; Dean and Arthur, 1998a; Scott et al., 1998). Interbedded (chalks) and marlstones in the Smoky Hill Chalk and the Bridge Creek Limestone produce extreme variation in percent $CaCO_3$ (ca. 40–90%). This is the result of dilution of carbonate by detrital clastic material derived from the Sevier volcanic highland on the western side of the WIS. The OC content is generally antithetic to that of $CaCO_3$ content in that the marlstone beds are enriched in the OC and the limestone/chalk beds are not.

Most of the organic matter in the Greenhorn, Carlile and Niobrara formations in the Amoco No. 1 Bounds core is well-preserved algal marine organic matter produced in the basin. The main exception is the Codell Sandstone Member of the Carlile Shale, which contains mainly Type III organic matter with a hydrogen index HI < 200 (Fig. 13). Terrestrial organic matter (Type III) typically has values of HI < 200, and well-preserved, algal marine organic matter (Type I and II) typically has values of HI > 400.

Carbonate in the Greenhorn and Niobrara formations was derived from calcareous nannoplankton (coccoliths), which were also the source of most of the organic matter. The coccoliths and the organic matter were rapidly delivered to the sea floor packaged in fecal pellets

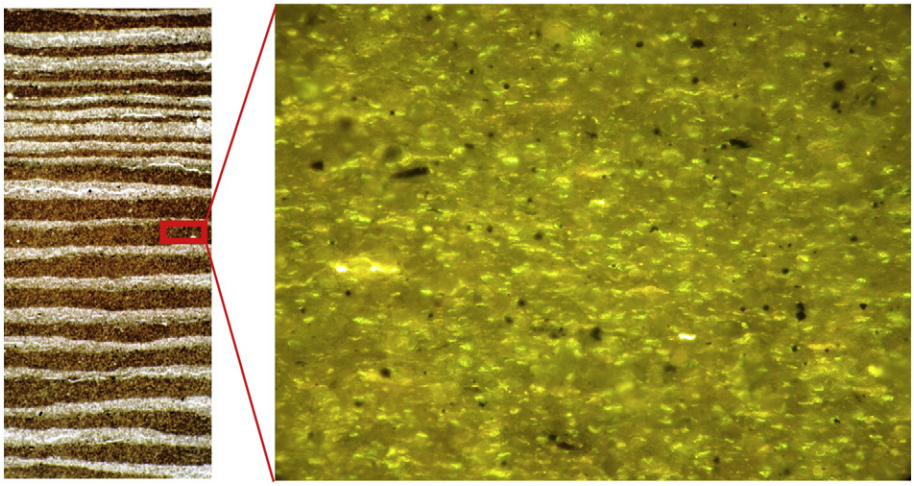

Fig. 12. Core and thin section showing lithologic and petrographic heterogeneity of source rock facies of member 1 of the Qingshankou Formation from a depth of 1245.59 m in the Chuan-5 well; organic-matter and dolomitic laminae intercalated (TOC content 3.9%; ×500 fluorescence microscopic picture).

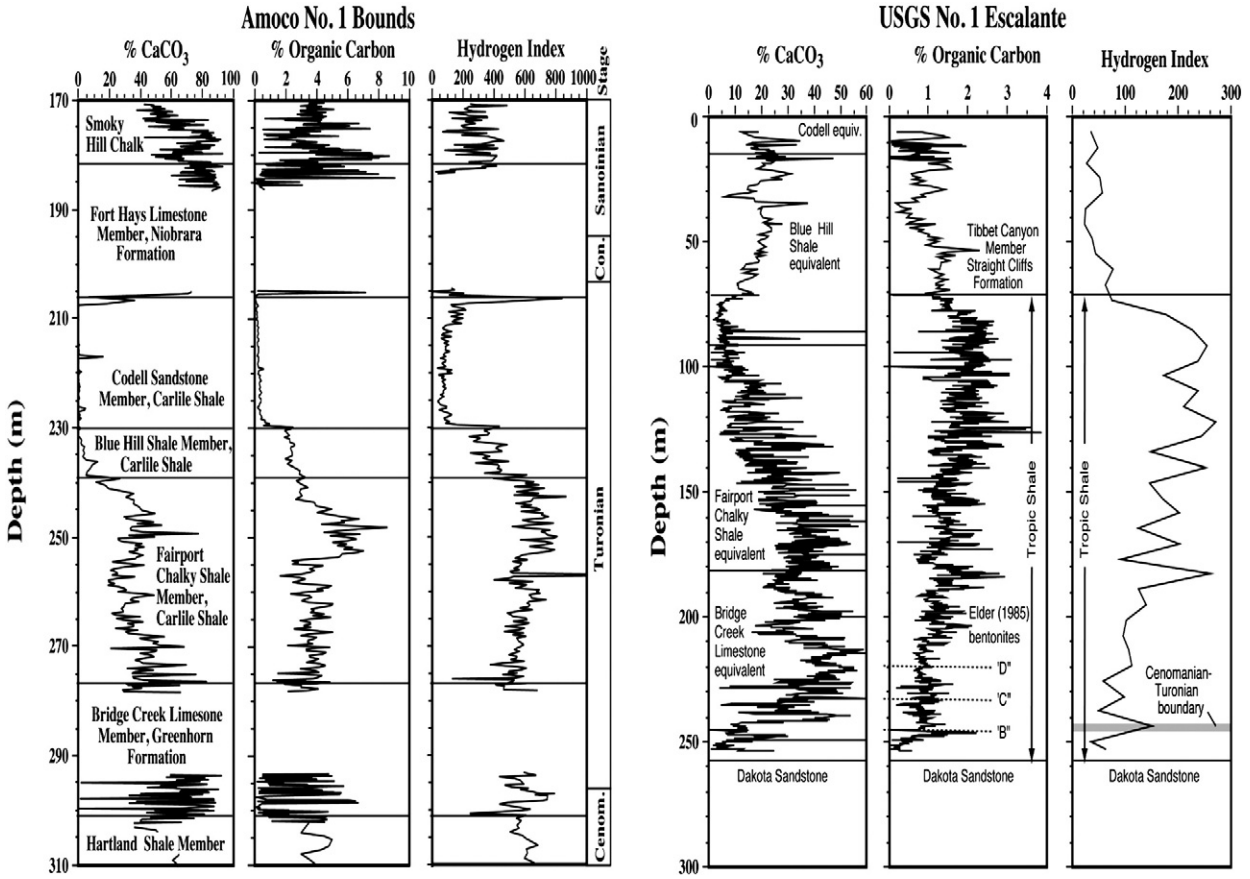

Fig. 13. Geochemical data of Cenomanian–Santonian stratigraphic units in basin center (Amoco No. 1 Bounds core) and western basin margin (USGS No. 1 Escalante core). Percent $CaCO_3$, percent organic carbon, and Rock–Eval pyrolysis hydrogen index for the Greenhorn and Niobrara formations in Bounds core are from Dean et al. (1995, fig. 7); data for the Carlile Shale (246–278 m) are from White and Arthur (2006). On western margin percent $CaCO_3$ of stratigraphic units in USGS No. 1 Escalante core are from Dean and Arthur (1998b, fig. 3), and percent organic carbon and Rock–Eval pyrolysis hydrogen index of units exposed on the Kaparowits Plateau are from Leithold (1993, 1994) and Leithold and Dean (1998, fig. 13). Bentonite marker beds "B", "C", "D" are from Elder (1985). Correlation of Tropic shale and Tibbet Canyon Member with basin-center units in eastern Colorado are indicated on $CaCO_3$ percent profile (left column). The Cenomanian–Turonian boundary is shown on the profile for hydrogen index.

that originated from herbivorous zooplankton (Hattin, 1971; Pratt et al., 1993). This rapid delivery of organic matter to anoxic bottom waters, through a relatively shallow, stratified water column, accounts for the preservation of amorphous, hydrogen-rich organic matter that is preserved in the marlstone beds (Pratt et al., 1993; Dean and Arthur, 1998b). These marlstones are now important hydrocarbon source rocks (e.g., Clayton and Swetland, 1980).

The climatic and oceanographic conditions of the north-to-south epicontinental WIS ranged from low-latitude humid to evaporitic conditions of the Tethys Ocean to the south, to high-latitude cool precipitation-dominated conditions of the Arctic Ocean to the north (e.g., Hay et al., 1993). Fluvial systems from the Sevier Highlands delivered terrigenous clastics with nutrients that fostered marine organic productivity. In addition, the extremely high biotic productivity in the WIS was fed by nutrient-rich, pre-conditioned, oxygen-depleted waters advected into the WIS from the Tethys Ocean (Arthur and Sageman, 2005; White and Arthur, 2006). Inflowing fresh water also produced salinity stratification of the basin with lower salinity surface waters and more saline, dysaerobic to anoxic bottom waters (Pratt et al., 1993).

Maximum transgression of the Cenomanian–Turonian Greenhorn cycle on the western margin of the Western Interior Basin deposited the Tropic Shale, which is time-equivalent of the Greenhorn Formation. The Tropic Shale is mainly a marlstone, with an average of 34% $CaCO_3$ and locally up to 60% (Fig. 13). The abundance of $CaCO_3$ in sediments deposited so close to the western margin of the WIS is further evidence that carbonate deposition occurred basin-wide and that variation in $CaCO_3$ in any one section, particularly in an east–west direction, is the result of clastic dilution. The Tropic Shale was deposited rapidly as fine-grained sediment in a prodeltaic environment (Leithold, 1993, 1994; Leithold and Dean, 1998). The biostratigraphy and abundant bentonite beds in the Tropic Shale permit correlation of $CaCO_3$ peaks with individual limestone beds in the Bridge Creek Limestone in the basin center (Laurin and Sageman, 2007; Dean et al., in press). Maximum transgression in the Tropic Shale during the Greenhorn cycle is represented in the Escalante core by the $CaCO_3$ maximum that is time-equivalent to the Bridge Creek Limestone in eastern Colorado and Kansas (Fig. 13). The progressive decrease in $CaCO_3$ content up section reflects the Greenhorn regression following maximum highstand.

The OC content of the Tropic Shale in the USGS No. 1 Escalante core generally increases upward from <1% to >3% (Fig. 13). This indicates that the amount of organic matter increased as the western shoreline of the WIS transgressed from east to west, and continued to increase during regression as shoreline and deltaic conditions prograded. The Rock–Eval pyrolysis hydrogen index (HI) indicates that most of the organic matter is terrestrial (Type III), which is to be expected considering the substantial influx of terrestrial clastic sediment to the WIS. However, values of HI in the Tropic Shale also generally increase upward parallel to the increase in OC (Fig. 13), suggesting that the proportion of algal marine organic matter increases up section. However, the amount of algal organic matter on the western margin was not nearly as great as in the basin center as indicated by the very high HI values in the Bridge Creek, Fairport, and Smoky Hill units in the Bounds core (Fig. 13). The increased algal marine organic matter of the Tropic Shale in the Escalante core was the response to OAE 2 during the Greenhorn transgressive–regressive cycle. However, the organic matter continues to increase up section past peak Greenhorn transgression, which indicates

local influx of terrestrial organic matter, and OC was not coupled to the Greenhorn transgression–regression cycle. However the $CaCO_3$ content represents basin-wide $CaCO_3$ production that was related to transgression (Fig. 13).

Values of ^{13}C in organic matter in the Tropic Shale at the Escalante core also are typical of those of Cretaceous terrestrial organic matter (e.g., coals; Dean et al., 1986), but at the Cenomanian–Turonian (C/T) boundary, values of ^{13}C show a positive excursion (^{13}C enrichment of up to 2‰; Dean et al., in press). A positive excursion is characteristic of values of ^{13}C in both carbonate and organic matter at the global C/T OAE 2 and was likely due to enhanced burial and preservation of ^{13}C-depleted organic matter enriching the entire carbon reservoir in ^{13}C (Schlanger et al., 1987; Arthur et al., 1988; Pratt et al., 1993). This is further evidence that the Tropic Shale core apparently records both global (OAE) and local events along the western shore of the WIS.

6.3. Comparison and discussion

Studies of modern and ancient lakes demonstrate that organic matter deposition in lakes differs from oceans in several significant ways (Fleet et al., 1988; Sladen, 1994). Lake systems are much more sensitive to changing accommodation space and climate than oceans because of their much smaller sediment and water volumes. Lake level and sediment supply are directly linked in lake systems; this contrasts greatly with marine systems, where sea level and sediment supply are only weakly linked at best and most models assume no linkage (e.g., Posamentier and Vail, 1988). These differences strongly influence the occurrence, distribution, and character of hydrocarbon source, reservoir, and seal play elements.

The age of organic deposition in both the SB and the WIS spans from Turonian to Santonian beginning with OAE 2 and ending during OAE 3 maximum transgression, although these anoxic events are not yet identified in the SB.

Organic matter types in the SB are mainly algal Types I and II deposited in shale rhythmites controlled by astronomically-driven climate cycles. Organic matter type in the WIS is both algal marine and terrestrial (Type III) deposited in limestone–marlstone cycles also driven by astronomical cycles. Productivity-dilution cyclicity was caused by variable terrigenous clastic influx from the west diluting marine carbonate. In the WIS nutrients were derived from both land and Tethyan water masses, but in the SB nutrients were mainly by terrestrial input.

Organic carbon deposition in the WIS resulted from stratification of cool, lower salinity Boreal water mass over warmer, higher salinity Caribbean water mass (Glancy et al., 1993; Hay et al, 1993). The periodic enhanced input of fresh water from the western mountain-highland of the seaway might have also caused marine stratification fostering organic carbon enriched marl/shale layers intercalated with carbonate (Fig. 14a). One evidence of this stratification is that oxygen isotopes of fossil shells in the organic carbon-rich layer is much lighter than that of carbonate (Pratt et al., 1993; Sageman et al., 1998). The input of freshwater might have been regulated by the orbital cycles (Sageman et al., 1998).

Bottom waters of the Songliao Lake experienced variable redox conditions and deposition of organic-rich sediments. Low oxygen, and fluctuating redox bottom water conditions (Wang et al., 2013) are indicated by the size distribution and morphology of single pyrite framboids in member 1 of the Qingshankou Formation (Wilkin and Barnes, 1996). One cause of anoxic to euxinic conditions may have been brief marine incursions indicated by marine microfossils. Different densities of fresh and marine waters would lead to stratification of the lake, and therefore buildup of bottom water anoxic conditions (Fig. 14b; Cohen, 2003).

In spite of the differences noted above, bottom water anoxia is the most favorable condition for organic carbon burial both in the SB and WIS basin regardless of its cause. Orbital forcings and coupling of geochemical cycles may also have regulated the burial of organic carbon in both realms.

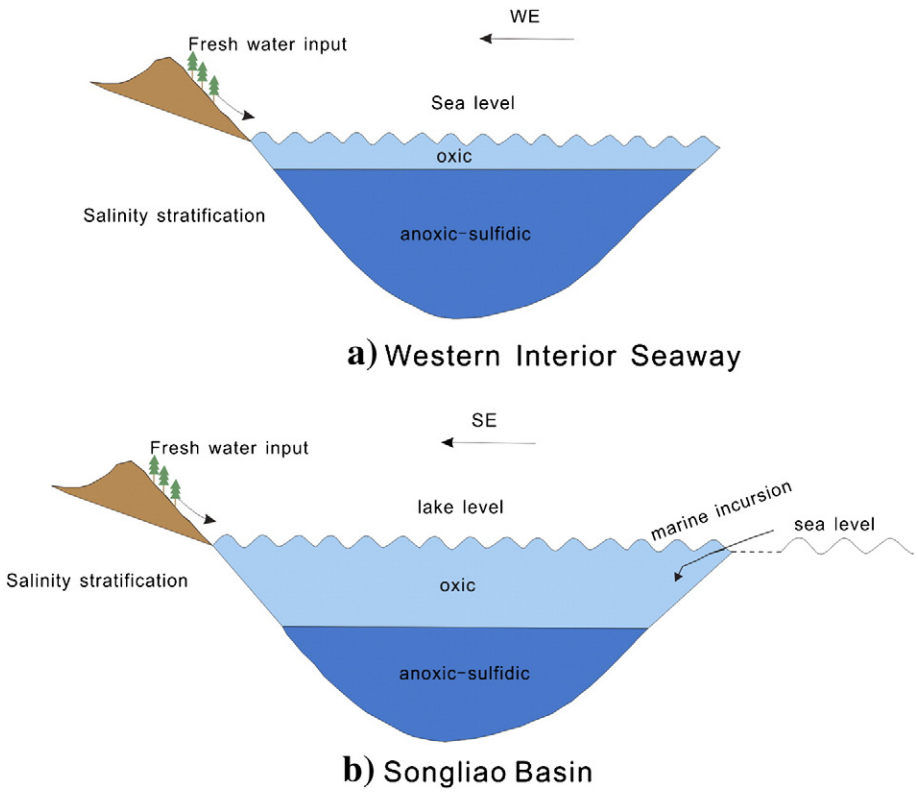

Fig. 14. Comparison of water column stratification model in Western Interior Seaway Basin (a) and Songliao Basin (b). See the text for details.

7. Summary

The data from Cretaceous rocks in the WIS and SB would seem to have important implications for understanding the greenhouse world as a whole. Continental and marine systems respond differently to global climate change. The dynamic Late Cretaceous climates of both the SB and WIS gradually cooled from the warmest Albian–Cenomanian time to the end of the Maastrichtian, which was consistent with the global trend. However the climate changes in the Songliao Basin were frequent and abrupt, whereas in the WIS climate change was more gradual because the seaway waters were a mixture of fresh-water runoff, warm Tethyan and cool Arctic waters. The long-term climate change in both terrestrial and marine systems was regulated by orbital forcing as evidenced by the sedimentary cycles in both sections. Cycles in the WIS and SB resulted from variations of the wet/dry runoff cycles responding to orbital forcing.

Organic-carbon-rich sediments were deposited in both basins during oceanic anoxic events. The organic carbon burial rate was much higher in the Songliao basin than in the WI suggesting that giant lakes may serve as important sinks of atmospheric CO_2. In both basins organic-rich deposits formed both during rising water levels and incursion of saline waters. Organic carbon-enriched sediments in both lakes and ocean absorbed excess CO_2 of the Cretaceous atmosphere.

Acknowledgments

We thank Mr. Timothy J. Horscroft and Mr. Paul B. Wignall for their encouragement and patient support in the process of preparing this manuscript. We are grateful for the support by ICDP and IGCP. We would like to thank B.B. Sageman, who helped clarify the discussion of the WIS Cenomanian–Turonian cyclostratigraphy. Thanks are also given to W.W. Hay and L.F. Jansa, who reviewed our manuscript and gave us many useful comments. We would like to thank the reviewers for the constructive comments. This study was financially supported by the National Basic Research Program of China (973 Project) grant no. 2012CB822000.

References

Allen, J.L., Johnson, C.L., 2011. Architecture and formation of transgressive–regressive cycles in marginal marine strata of the John Henry Member, Straight Cliffs Formation, Upper Cretaceous of Southern Utah, USA. Sedimentology 58, 1486–1513.

Amiot, R., Lécuyer, C., Buffetaut, E., Fluteau, F., Legendre, S., Martineau, F., 2004. Latitudinal temperature gradient during the Cretaceous Upper Campanian–Middle Maastrichtian: $\delta^{18}O$ record of continental vertebrates. Earth Planet. Sci. Lett. 226, 255–272.

Ando, A., Huber, B.T., MacLeod, K.G., Tomoko, O., Boo-Keun, K., 2009. Blake Nose stable isotopic evidence against the mid-Cenomanian glaciation hypothesis. Geology 37, 451–454.

Armstrong, R.L., Ward, P.L., 1993. Late Triassic to earliest Eocene magmatism in the North American Cordillera: implications for the Western Interior Basin. In: Caldwell, W.G.E., Kauffman, E.G. (Eds.), Evolution of the Western Interior BasinGeol. Assoc. Can. Spec. Pap. 39, 49–72.

Arthur, M.A., Sageman, B.B., 2005. Sea-level control on source-rock development: perspectives from the Holocene Black Sea, the mid-Cretaceous Western Interior Basin of North America, and the Late Devonian Appalachian Basin. In: Harris, N., Pradier, B. (Eds.), The Deposition of Organic-Rich Sediments: Models, Mechanisms, and ConsequencesSEPM Spec. Publ. 82, 35–59.

Arthur, M.A., Schlanger, S.O., 1979. Cretaceous 'oceanic anoxic events' as causal factors in development of reef-reservoired giant oil fields. AAPG Bull. 63, 870–885.

Arthur, M.A., Dean, W.E., Bottjer, D.A., Scholle, P.A., 1984. Rhythmic bedding in Mesozoic–Cenozoic pelagic carbonate sequences; the primary and diagenetic origin of Milankovitch-like cycles. In: Berger, A., Imbrie, J., Hays, J.D., Kukla, G., Saltzman, B. (Eds.), Milankovitch and Climate, pt. 1. Reidel Publishing Co., Amsterdam, pp. 191–222.

Arthur, M.A., Schlanger, S.O., Jenkyns, H.C., 1987. The Cenomanian–Turonian oceanic anoxic event, II. Paleoceanographic controls on organic matter production and preservation. In: Brooks, J., Fleet, A. (Eds.), Marine Petroleum Source RocksGeol. Soc. Lond. Spec. Publ. 26, 401–420.

Arthur, M.A., Dean, W.E., Pratt, L.M., 1988. Geochemical and climatic effects of increased organic carbon burial at the Cenomanian/Turonian boundary. Nature 335, 714–717.

Arthur, M.A., Brumsack, H.J., Jenkyns, H.C., Schlanger, S.O., 1990. Stratigraphy, geochemistry, and paleoceanography of organic carbon-rich Cretaceous sequences. In: Ginsburg, R.N., Beaudoin, B. (Eds.), Cretaceous, Resources, Events, and Rhythms: Background and Plans for Research. Kluwer Academic Publishers, Dordrecht, the Netherlands, pp. 75–119.

Barrera, E., Savin, S.M., 1999. Evolution of late Campanian–Maastrichtian marine climates and oceans. In: Barrera, E., Johnson, C. (Eds.), Evolution of the Cretaceous Ocean-Climate SystemGeol. Soc. Am. Spec. Pap. 332, 245–282.

Bechtel, A., Jia, J.L., Strobl, S.A.I., Sachsenhofer, R.F., Liu, Z.J., Gratzer, R., Püttmann, W., 2012. Palaeoenvironmental conditions during deposition of the Upper Cretaceous oil shale sequences in the Songliao Basin (NE China): implications from geochemical analysis. Org. Geochem. 46, 76–95.

Bergman, K.M., Walker, R.G., 1999. Campanian Shannon Sandstone: an example of a falling stage systems tract deposit. In: Bergman, K.M., Snedden, J.W. (Eds.), Isolated Shallow Marine Sand Bodies: Sequence Stratigraphic Analysis and Sedimentologic InterpretationSEPM Spec. Publ. 64, 85–93.

Bohor, B.F., Triplehorn, D.M., Nichols, D.J., Millard, H.T., 1987. Dinosaurs, spherules, and the "majic" layer: a new K-T boundary clay site in Wyoming. Geology 15, 896–899.

Boucot, A.J., Chen, X., Scotese, C.R., Fan, J.X., 2009. Reconstruction of Global Paleoclimate in Phanerozoic. Science Press, Beijing (in Chinese).

Burns, C.E., Bralower, T.J., 1998. Upper Cretaceous nannofossil assemblages across the Western Interior seaway: implications for the origins of lithologic cycles in the Greenhorn and Niobrara formations. In: Dean, W.E., Arthur, M.A. (Eds.), Stratigraphy and paleoenvironments of the Cretaceous Western Interior seaway, USA. SEPM Concepts in Sedimentology and Paleontology, 6, pp. 35–58.

Burtner, R.L., Warner, M.A., 1984. Hydrocarbon generation in the lower Cretaceous Mowry and Skull Creek Shales of the northern Rocky Mountain area. In: Woodward, J., Meissner, J.L., Clayton, J.L. (Eds.), Hydrocarbon Source Rocks of the Greater Rocky Mountain Region. Rocky Mountain Association of Geologists Guidebook, pp. 449–467.

Bush, A.B.G., Philander, S.G.H., 1997. The late Cretaceous: simulation with a coupled atmosphere–ocean general circulation model. Paleoceanography 12, 495–516.

Cadrin, A.A.J., Kyser, T.K., Caldwell, W.G.E., Longstaffe, F.J., 1996. Isotopic and chemical compositions of bentonites as paleoenvironmental indicators of the Cretaceous Western Interior Seaway. Palaeogeogr. Palaeoclimatol. Palaeoecol. 119, 301–320.

Caraco, N.F.J., Cole, J., Likens, G.E., 1993. Sulfate control of phosphorus availability in lakes: a test and re-evaluation of Hasler and Einsele's Model. Hydrobiologia 253, 275–280.

Caron, M., Dall'Agnolo, S., Accarie, H., Barrera, E., Kauffman, E.G., Amédro, F., Robaszynski, F., 2006. High-resolution stratigraphy of the Cenomanian–Turonian boundary interval at Pueblo (USA) and wadi Bahloul (Tunisia): stable isotope and bio-events correlation. Géobios 39, 171–200.

Chamberlain, C.P., Wan, X.Q., Graham, S.A., Carroll, A.R., Doebbert, A.C., Sageman, B.B., Blisniuk, P., Kent-Corson, M.L., Wang, Z., Wang, C.S., 2013. Stable isotopic evidence for climate and basin evolution of the Late Cretaceous Songliao basin, China. Palaeogeogr. Palaeoclimatol. Palaeoecol. 385, 106–124.

Chen, P.J., 1987. Cretaceous paleogeography of China. Palaeogeogr. Palaeoclimatol. Palaeoecol. 59, 49–56.

Chen, P.J., Chang, Z.L., 1994. Nonmarine Cretaceous stratigraphy of eastern China. Cretac. Res. 5, 245–257.

Chen, J.M., Zhao, P., Wang, C.S., Huang, Y.J., Cao, K., 2013. Modeling East Asian climate and impacts of atmospheric CO_2 concentration during the Late Cretaceous (66 Ma). Palaeogeogr. Palaeoclimatol. Palaeoecol. 385, 190–201.

Cheng, R.H., Wang, G.D., Wang, P.J., 2008. Sedimentary cycles of the Cretaceous Quantou–Nenjiang Formations and Milankovitch cycles of the South Hole of the SLCORE-I in the Songliao Basin. Acta Geol. Sin. (Chin. Ed.) 82, 55–64 (in Chinese with English abstract).

Cheng, R.H., Wang, G.D., Wang, P.J., Gao, Y.F., Ren, Y.G., Wang, C.S., Zhang, S.H., Wang, Q.Y., 2009. Description of Cretaceous sedimentary sequence of the Yaojia Formation recovered by CCSD-SK-Is borehole in Songliao Basin: lithostratigraphy, sedimentary facies and cyclic stratigraphy. Earth Sci. Front. 16 (2), 272–287.

Clayton, J.L., Swetland, P.J., 1980. Petroleum generation and migration in Denver Basin. AAPG Bull. 64, 1613–1633.

Cobban, W.A., 1993. Diversity and distribution of Late Cretaceous ammonites, Western Interior, United States. In: Caldwell, W.G.E., Kauffman, E.G. (Eds.), Evolution of the Western Interior BasinGeol. Assoc. Can. Spec. Pap. 39, 435–452.

Cobban, W.A., Walaszczyk, I., Obradovich, J.D., McKinney, K.C., 2006. A USGS Table for the Upper Cretaceous Middle Cenomanian–Maastrichtian of the Western Interior of the United States based on ammonites, inoceramids, and radiometric ages. U.S. Geological Survey Open-file report 2006-1250 (45 pp.).

Cochran, J.K., Landman, N.H., Turekian, K.K., Michar, A., Schrag, D.P., 2003. Paleoceanography of the Late Cretaceous (Maastrichtian) Western Interior Seaway of North America: evidence from Sr and O isotopes. Palaeogeogr. Palaeoclimatol. Palaeoecol. 191 (1), 45–64. http://dx.doi.org/10.1016/S0031-0182(02)0042-9.

Cohen, A.S., 2003. Paleolimnology: The History and Evolution of Lake Systems. Oxford University Press (528 pp.).

Cook, T.D., Bally, A.W., 1975. Stratigraphic atlas of North and Central America: Princeton. Princeton University Press, New Jersey (272 pp.).

Coulson, A.B., Kohn, M.J., Barrick, R.E., 2011. Isotopic evaluation of ocean circulation in the Late Cretaceous North American seaway. Nat. Geosci. 4, 852–855.

Cramer, B.S., Toggweiler, J.R., Wright, J.D., Katz, M.E., Miller, K.G., 2009. Ocean overturning since the Late Cretaceous: inferences from a new benthic foraminiferal isotope compilation. Paleoceanography 24, PA4216.

Dean, W.E., Arthur, M.A., 1998a. Cretaceous Western Interior seaway drilling project: an overview. In: Dean, W.E., Arthur, M.A. (Eds.), Stratigraphy and Paleoenvironments of the Cretaceous Western Interior seaway, USA. SEPM Concepts in Sedimentology and Paleontology, 6, pp. 1–10.

Dean, W.E., Arthur, M.A., 1998b. Geochemical expressions of cyclicity in Cretaceous pelagic limestone sequences: Niobrara Formation, Western Interior seaway. In: Dean, W.E., Arthur, M.A. (Eds.), Stratigraphy and Paleoenvironments of the

Cretaceous Western Interior Seaway. USA SEPM Concepts in Sedimentology and Paleontology, 6, pp. 227–255.
Dean, W.E., Arthur, M.A., Claypool, G.E., 1986. Depletion of 13C in Cretaceous marine organic matter—source, diagenetic, or environmental signal? Mar. Geol. 70, 119–157.
Dean, W.E., Arthur, M.A., Sageman, B.B., Lewan, M.D., 1995. Core descriptions and preliminary geochemical data for the Amoco Production Company Rebecca K. Bounds #1 well, Greeley County, Kansas. U.S. Geological Survey Open-File Report 95-209 (243 pp.).
Dean, W.E., Kauffman, E.G., Arthur, M.A., 2013. Accumulation of organic-carbon-rich strata along the western margin and in the center of the North American Cretaceous Western Interior Seaway during the Cenomanian–Turonian transgression. In: Titus, A.L., Loewen, M.A. (Eds.), Late Cretaceous Geology and Paleontology of the Grand Staircase, Southern Utah: Critical Window Into End-Mesozoic Ecosystems. Indiana University Press (in press).
DeCelles, P.G., 1994. Late Cretaceous–Paleocene synorogenic sedimentation and kinematic history of the Sevier thrust belt, northeast Utah and southwest Wyoming. Geol. Soc. Am. Bull. 106, 32–56.
DeCelles, P.G., Giles, K.N., 1996. Foreland basin systems. Basin Res. 8, 105–123.
DeCelles, P.G., Lawton, T.F., Mitra, G., 1995. Thrust timing, growth of structural culminations, and synorogenic sedimentation in the type Sevier orogenic belt, western United States. Geology 23, 699–702.
DeConto, R.M., Hay, W.W., Thompson, S.L., Bergengren, J., 1999. Late Cretaceous climate and vegetation interactions: cold continental interior paradox. In: Barrera, C.C., Johnson, M. (Eds.), Evolution of the Cretaceous ocean-climate systemGeol. Soc. Am. Spec. Pap. 332, 391–406.
Deng, C.L., He, H.Y., Pan, Y.X., Zhu, R.X., 2013. Chronology of the terrestrial Upper Cretaceous in Songliao Basin, northeast Asia. Palaeogeogr. Palaeoclimatol. Palaeoecol. 385, 44–54.
Dennis, K.J., Cochran, J.K., Landman, N.H., Schrag, D.P., 2013. The climate of the Late Cretaceous: new insights from the application of the carbonate clumped isotope thermometer to Western Interior Seaway macrofossil. Earth Planet. Sci. Lett. 362, 51–65.
Dickinson, W.R., Snyder, W.S., 1978. Plate tectonics of the Laramide orogeny. In: Matthews, V. (Ed.), Laramide Folding Associated With Block Faulting in the Western United StatesGeol. Soc. Am. Mem. 151, 355–366.
Donnadieu, Y., Godderis, Y., Bouttes, N., 2009. Exploring the climatic impact of the continental vegetation on the Mezosoic atmospheric CO2 and climate history. Clim. Past 5, 85–96.
Dworkin, S.I., Nordt, L., Atchley, S., 2005. Determining terrestrial paleotemperatures using the oxygen isotopic composition of pedogenic carbonate. Earth Planet. Sci. Lett. 237, 56–68.
Eicher, D.L., Diner, R., 1989. Origin of the Cretaceous Bridge Creek cycles in the Western Interior, United States. Palaeogeogr. Palaeoclimatol. Palaeoecol. 74, 127–146.
Elder, W.P., 1985. Biotic patterns across the Cenomanian–Turonian extinction boundary near Pueblo, Colorado. In: Pratt, L.M., Kauffman, E.G., Zelt, F.B. (Eds.), Fine-grained Deposits and Biofacies of the Cretaceous Western Interior Seaway: Evidence of Cyclic Sedimentary Processes. SEPM Society of Economic Paleontologists and Mineralogists, 1985 Midyear Meeting, Golden, Colorado, Field Trip Guidebook, 4, pp. 157–169.
Feng, Z.Q., Huo, Q.L., Wang, X., Fang, W., Song, Z.G., 2009. Geochemical research on the Late Cretaceous strata of Well SK1 in Songliao Basin. Earth Sci. Front. 16 (5), 181–191.
Feng, Z.Q., Jia, C.Z., Xie, X.N., Zhang, S., Feng, Z.H., Cross, T.A., 2010. Tectonostratigraphic units and stratigraphic sequences of the nonmarine Songliao basin, northeast China. Basin Res. 22, 79–95.
Finn, T.M., 2010. New source rock data for the Thermopolis and Mowry Shales in the Wyoming part of the Bighorn Basin. U.S. Geological Survey Digital Data Series DDS-69-V (16 pp.).
Fleet, A.J., Kelts, K., Talbot, M., 1988. Lacustrine petroleum source rocks. Geol. Soc. Spec. Pub. 40, 1–391.
Flögel, S., Parkin, G., Pollard, D., Dullo, W.-C., Wagner, T., 2011a. Simulating zonal scale shifts in the partitioning of surface and subsurface freshwater flow in response to increasing pCO_2. Climate Dynam. 37, 1565–1573.
Flögel, S., Wallmann, K., Kuhnt, W., 2011b. Cool episodes in the Cretaceous—exploring the effects of physical forcings on Antarctic snow accumulation. Earth Planet. Sci. Lett. 307, 279–288.
Fricke, H.C., Foreman, B.Z., Sewall, J.O., 2010. Integrated climate model-oxygen isotope evidence for a North American monsoon during the Late Cretaceous. Earth Planet. Sci. Lett. 289, 11–21.
Friedrich, O., Norris, R.D., Erbacher, J., 2012. Evolution of middle to Late Cretaceous oceans—A 55 m.y. record of Earth's temperature and carbon cycle. Geology 40 (2), 107–110.
Gächter, R., Müller, B., 2003. Why the phosphorus retention of lakes does not necessarily depend on the oxygen supply to their sediment surface. Limnol. Oceanogr. 48, 929–933.
Gale, A.S., Hardenbol, J., Hathway, B., Kennedy, J.W., Young, J.R., Phanskalar, V., 2002. Global correlation of Cenomanian (Upper Cretaceous) sequences: evidence for Milankovitch control on sea level. Geology 30, 291–294.
Gale, A.S., Voight, S., Sageman, B.B., Kennedy, W.J., 2008. Eustatic sea-level record for the Cenomanian (Late Cretaceous)—extension to the Western Interior Basin, USA. Geology 36, 859–862.
Gao, R.Q., Zhang, Y., Cui, T.C., 1994. Cretaceous Petroleum Bearing Strata in the Songliao Basin. Petroleum Industry Press, Beijing (1–333 pp. (in Chinese with English abstract)).
Gao, R.Q., Zhao, C.B., Qiao, X.Y., Zheng, Y.L., Yan, F.Y., Wan, C.B., 1999. Cretaceous Oil Strata Palynology from Songliao Basin. Geological Publishing House, Beijing (in Chinese).
Gao, Y.F., Wang, P.J., Cheng, R.H., Wang, G.D., Wan, X.Q., Wu, H.Y., Wang, S.X., Liang, W.L., 2009. Description of Cretaceous sedimentary sequence of the first member of the Qingshankou Formation recovered by CCSD-SK-I s borehole in Songliao Basin: lithostratigraphy, sedimentary facies and cyclic stratigraphy. Earth Sci. Front. 16, 314–323 (in Chinese with English abstract).
Gao, X., Wang, P.K., Li, Q.Y., Wang, C.S., Gao, Y., 2010. The precise naming and mineralogical characteristics of ferruginous lacustrine dolomite in well CCSD-SK. Acta Petrol. Mineral. 29, 213–218.
Gardner, M.H., 1995. Tectonic and eustatic controls on the stratal architecture of mid-Cretaceous stratigraphic sequences, central western interior foreland basin of North America. In: Steininger, R., Pennell, B. (Eds.), Stratigraphic Evolution of Foreland BasinsSEPM Spec. Publ. 52, 243–279.
Gardner, H.M., Cross, T.A., 1994. Middle Cretaceous paleogeography of Utah. In: Caputo, M.V., Peterson, J.A., Franczyk, K.J. (Eds.), Mesozoic Systems of the Rocky Mountain region, USA. SEPM Society of Economic Mineralogists and Paleontologists, Rocky Mountain Section, pp. 471–502.
Gilder, S., Courtillot, V., 1997. Timing of the North–South China collision from new middle to late Mesozoic paleomagnetic data from the North China Block. J. Geophys. Res. 102, 17713–17727.
Gill, J.R., Cobban, W.A., 1966. The Red Bird section of Upper Cretaceous Pierre Shale in Wyoming. U.S. Geological Survey Professional Paper 393-A. (73 pp.).
Glancy Jr., T.J., Arthur, M.A., Barron, E.J., Kauffman, E.G., 1993. A paleoclimate model for the North American Cretaceous (Cenomanian–Turonian) epicontinental sea. In: Caldwell, W.G.E., Kauffman, E.G. (Eds.), Evolution of the Western Interior BasinGeol. Assoc. Can. Spec. Pap. 39, 219–241.
Golozubov, V., Malinovsky, A.I., Simanenko, V.P., 2006. About tektoncheskih reconstruction of Sikhote–Alin-level East Asian okrayny: there may be a simple solution. Pac. Geol. 25 (4), 115–119.
Gordon, W.A., 1973. Marine life and ocean surface currents in the Cretaceous. J. Geol. 81, 269–284.
Gradstein, F.M., Ogg, J.G., Smith, A.G., 2004. A Geologic Time Scale 2004. Cambridge University Press, Cambridge 1–589.
Graham, S.A., et al., 1987. Provenance modeling as a technique for analyzing source terrane evolution and controls on foreland sedimentation. Int. Assoc. Sedimentol. Spec. Publ. 8, 425–436.
Graham, S.A., Hendrix, M.S., Badarch, G., Badamgarav, D., 1996. Sedimentary record of transition from contractile to extensional tectonism, Mesozoic, southern Mongolia. Geol. Soc. Am. Abstr. Programs 28, A-68.
Graham, S.A., Hendrix, M.S., Jonson, C.L., Badamgarav, D., Badarch, G., Amory, J., Porter, M., Barsbold, R., Webb, L.E., Hacker, B.R., 2001. Sedimentary record and tectonic implications of Mesozoic rifting in southeast Mongolia. Geol. Soc. Am. Bull. 113, 1560–1579.
Haggart, J.W., Matsukawa, M., Ito, M., 2006. Paleogeographic and paleoclimatic setting of Lower Cretaceous basins of East Asia and western North America, with reference to the nonmarine strata. Cretac. Res. 27, 149–167.
Hancock, J.M., Walaszczyk, I., 2004. Mid-Turonian to Coniacian changes of sea level around Dallas, Texas. Cretac. Res. 25, 459–471.
Hancock, J.M., Kennedy, W.J., Cobban, W.A., 1993. A correlation of the Upper Albian to basal Coniacian sequences of northwest Europe, Texas and the United States Western Interior. In: Caldwell, W.G.E., Kauffman, E.G. (Eds.), Evolution of the Western Interior BasinGeol. Assoc. Can. Spec. Pap. 39, 453–476.
Hattin, D.E., 1971. Widespread synchronously deposited burrow-mottled limestone beds in the Greenhorn Limestone (Upper Cretaceous) of Kansas and southeastern Colorado. AAPG Bull. 55, 412–431.
Hay, W.W., 2008. Evolving ideas about the Cretaceous climate and ocean. Cretac. Res. 29, 725–753.
Hay, W.W., 2009. Cretaceous oceans and ocean modeling. In: Wang, C., Hu, X., Scott, R.W., Wagriech, M., Jansa, L. (Eds.), Cretaceous Oceanic Red Beds: Stratigraphy, Composition, Origins, and Paleoceanographic and Paleoclimatic SignificanceSEPM Spec. Publ. 91, 232–271.
Hay, W.W., 2011. Can humans force a return to a 'Cretaceous' climate? Sediment. Geol. 235, 5–26.
Hay, W.W., Eicher, D.L., Diner, R., 1993. Physical oceanography and water masses in the Cretaceous Western Interior Seaway. In: Dean, W.E., Arthur, M.A. (Eds.), Stratigraphy and Paleoenvironments of the Cretaceous Western Interior Seaway. SEPM (Society for Sedimentary Geology) Concepts in Sedimentology and Paleontology, 6, pp. 297–318.
He, S., Kyser, T.K., Caldwell, W.G.E., 2005. Paleoenvironment of the Western Interior Seaway inferred from $\delta^{18}O$ and $\delta^{13}C$ values of molluscs from the Cretaceous Bearpaw marine cyclothem. Palaeogeogr. Palaeoclimatol. Palaeoecol. 217, 67–85.
He, H.Y., Deng, C.L., Wang, P.J., Pan, Y.X., Zhu, R.X., 2012. Toward age determination of the termination of the Cretaceous normal superchron. Geochem. Geophys. Geosyst. 13 (1), Q02002. http://dx.doi.org/10.1029/2011GC003901.
Hendrix, M.S., Davis, G.A., 2001. Paleozoic and Mesozoic tectonic evolution of central and eastern Asia: from continental assembly to intracontinental deformation. Geol. Soc. Am. Mem. 194, 447pp.
Hicks, J.F., Obradovich, J.D., Tauxe, L., 1999. Magnetostratigraphy, isotopic age calibration and intercontinental correlation of the Red Bird section of the Pierre Shale, Niobrara County, Wyoming, USA. Cretac. Res. 20, 1–27.
Higley, D.K., Cox, D.O., 2007. Oil and gas exploration and development along the Front Range in the Denver Basin of Colorado, Nebraska, and Wyoming. In: Higley, D.K. (Compiler), Petroleum systems and assessment of undiscovered oil and gas in the Denver Basin Province, Colorado, Nebraska, Kansas, South Dakota and Wyoming-USGS province 39. U.S. Geological Survey Digital Data Series DDS-69-P, ch. 2, (41 pp.).
Hinnov, L.A., Hilgen, F.J., 2012. Cyclostratigraphy and astrochronology. In: Gradstein, F.M., Ogg, J.G., Schmitz, M., Ogg, G. (Eds.), The Geologic Time Scale 2012. Elsevier, pp. 63–83.
Holbrook, J.M., Scott, R.W., Oboh-Ikuenobe, F.E., 2006. Base-level buffers and buttresses: a model for upstream and downstream control on fluvial geometry and architecture within sequences. J. Sediment. Res. 76, 162–174.

Hou, D.J., Li, M.W., Huang, Q.H., 2000. Marine transgressional events in the gigantic freshwater lake Songliao: paleontological and geochemical evidence. Org. Geochem. 31, 763–768.
Hu, X.M., Wagreich, M., Yilmaz, I.O., 2012. Marine rapid environmental/climatic change in the Cretaceous greenhouse world. Cretac. Res. 38, 1–6.
Huang, F.T., Huang, Q.H., 1998. Rhythm of geological events and interaction of different geospheres in Mesozoic of Songliao Basin. Pet. Explor. Dev. 25, 86–89 (in Chinese with English Abstracts).
Huang, Y.J., Yang, G.S., Gu, J., Wang, P.K., Huang, Q.H., Feng, Z.H., Feng, L.J., 2013. Marine incursion events in the Late Cretaceous Songliao Basin: constraints from sulfur geochemistry records. Palaeogeogr. Palaeoclimatol. Palaeoecol. 385, 152–161.
Huber, B.T., Hodell, D.A., Hamilton, C.P., 1995. Mid- to Late Cretaceous climate of the southern high latitudes: stable isotopic evidence for minimal equator-to-pole thermal gradients. Geol. Soc. Am. Bull. 107, 392–417.
Husson, D., Galbrun, B., Laskar, J., Hinnov, L.A., Thibault, N., Gardin, S., Locklair, R.E., 2011. Astronomical calibration of the Maastrichtian (Late Cretaceous). Earth Planet. Sci. Lett. 305, 328–340.
Ishida, K., Kozai, T., Park, S.O., Mitsugi, T., 2003. Gravel bearing radiolaria as tracers for erosional events: a review of the status of recent research in SW Japan and Korea. J. Asian Earth Sci. 21 (8), 909–920.
Jenkyns, H.C., 1980. Cretaceous anoxic events-from continents to oceans. J. Geol. Soc. Lond. 137, 171–188.
Jenkyns, H.C., Mutterlose, J., Sliter, W.V., 1995. Upper Cretaceous carbon- and oxygen-isotope stratigraphy of deep-water sediments from the north-central Pacific (Site 869, Flank of Pikinni-Wodejebato, Marshal Islands). In: Winterer, E.L., Sager, W.W., Firth, J.V., Sinton, J.M. (Eds.), Proc. Ocean Drill. Program Sci. Results 143, 105–108.
Jordan, T., 1995. Retroarc foreland and related basins. In: Busby, C.J., Ingersoll, R.V. (Eds.), Tectonics of Sedimentary Basins. Blackwell Science, pp. 331–362.
Kauffman, E.G., 1977. Geological and biological overview: Western Interior Cretaceous Basin. In: Kauffman, E.G. (Ed.), Cretaceous Facies. Faunas and Paleoenvironments across the Western Interior Basin, Mountain Geologist, 14, pp. 75–99.
Kauffman, E.G., 1984. Paleobiogeography and evolutionary response dynamic in the Cretaceous Western Interior seaway of North America. In: Westermann, G.E.G. (Ed.), Jurassic–Cretaceous Biochronology and Paleogeography of North AmericaGeol. Assoc. Can. Spec. Pap. 27, 275–306.
Kauffman, E.G., Caldwell, W.G.E., 1993. The Western Interior Basin in space and time. In: Caldwell, W.G.E., Kauffman, E.G. (Eds.), Evolution of the Western Interior BasinGeol. Assoc. Can. Spec. Pap. 39, 1–30.
Kauffman, E.G., Sageman, B.B., Kirkland, J.I., Elder, W.P., Harries, P.J., Villamil, T., 1993. Molluscan biostratigraphy of the Cretaceous Western Interior Basin, North America. In: Caldwell, W.G.E., Kauffman, E.G. (Eds.), Evolution of the Western Interior BasinGeol. Assoc. Can. Spec. Pap. 39, 397–434.
Keller, G., Berner, Z., Adatte, T., Stueben, D., 2004. Cenomanian–Turonian and $\delta^{13}C$, and $\delta^{18}O$, sea level and salinity variations at Pueblo, Colorado. Palaeogeogr. Palaeoclimatol. Palaeoecol. 211, 19–43.
Klinger, H.C., Kakabadze, M.V., Kennedy, W.J., 1984. Upper Barremian (Cretaceous) heteroceratid ammonites from South Africa and the Caucasus and their palaeobiogeographic significance. J. Molluscan Stud. 50, 43–60.
Laferriere, L., 1992. Regional isotopic variations in the Fort Hays Member of the Niobrara Formation, United States Western Interior: primary signals and diagenetic overprinting in a Cretaceous pelagic rhythmite. Geol. Soc. Am. Bull. 104, 980–992.
LaFerriere, A.P., Hattin, D., Archer, A.W., 1987. Effects of climate, tectonics and sea-level changes on rhythmic bedding patterns in the Niobrara Formation (Upper Cretaceous), U.S., Western Interior. Geology 15, 233–236.
Lanci, L., Muttoni, G., Erba, E., 2010. Astronomical tuning of the Cenomanian Scaglia Bianca Formation at Furlo, Italy. Earth Planet. Sci. Lett. 292, 231–237.
Laskar, J., Fienga, A., Gastineau, M., Manche, H., 2011. A new orbital solution for the long term motion of the Earth. Astron. Astrophys. 532. http://dx.doi.org/10.1051/0004-6361/201116836.
Laurin, J., Sageman, B.B., 2007. Cenomanian–Turonian coastal record in SW Utah, U.S.A.: orbital-scale transgressive–regressive events during Oceanic Anoxic Event II. J. Sediment. Res. 77, 731–756.
Lawton, T., 1986. Compositional trends within a clastic wedge adjacent to a fold–thrust belt: Indianola Group, central Utah, U.S.A. In: Allen, P.A., Homewood, P. (Eds.), Foreland BasinsInt. Assoc. Sedimentol. Spec. Publ. 8, 411–423.
Leckie, R.M., Salacup, J.M., Petsch, S.T., 2008. Oceanic Anoxic Event 3 (Coniacian–Santonian, Late Cretaceous) in the Western Interior Seaway. Geol. Soc. Am. Abstr. Programs 40 (6), 238.
Leithold, E.L., 1993. Preservation of laminated shale in ancient clinoforms. Comparison to modern subaqueous deltas. Geology 21, 359–362.
Leithold, E.L., 1994. Stratigraphical architecture at the muddy margin of the Cretaceous Western Interior Seaway, southern Utah. Sedimentology 41, 521–542.
Leithold, E.L., Dean, W.E., 1998. Depositional processes and carbon burial on a Turonian prodelta at the margin of the Western Interior Seaway. In: Dean, W.E., Arthur, M.A. (Eds.), Stratigraphy and Paleoenvironments of the Cretaceous Western Interior Seaway. USA SEPM Concepts in Sedimentology and Paleontology, 6, pp. 189–200.
Li, H.Y., Zhang, S.H., Wu, H.C., Zhao, K.L., Yang, T.S., Zhao, L., 2013. Rock magnetic records of the Qingshankou Formation of SK-1 south borehole in Songliao Basin, Northeast China, and their paleoclimate implications. Palaeogeogr. Palaeoclimatol. Palaeoecol. 385, 71–82.
Locklair, R.E., Sageman, B.B., 2008. Cyclostratigraphy of the Upper Cretaceous Niobrara Formation, Western Interior, U.S.A.: a Coniacian–Santonian orbital timescale. Earth Planet. Sci. Lett. 269, 540–553.
McArthur, J.M., Kennedy, W.J., Chen, M., Thirlwall, M.F., Gale, A.S., 1994. Strontium isotope stratigraphy for Late Cretaceous time: direct numerical calibration of the Sr isotope curve based on the US Western Interior. Palaeogeogr. Palaeoclimatol. Palaeoecol. 108, 95–119.
Merewether, E.A., Cobban, W.A., Obradovich, J.D., 2007. Regional disconformities in Turonian and Coniacian (Upper Cretaceous) strata in Colorado, Wyoming, and adjoining states—biochronological evidence. Rocky Mt. Geol. 42 (2), 95–122.
Metelkin, D.V., Gordienko, I.V., Klimuk, V.S., 2007. Paleomagnetism of Upper Jurassic basalts from Transbaikalia: new data on the time of closure of the Mongol–Okhotsk Ocean and Mesozoic intraplate tectonics of Central Asia. Russ. Geol. Geophys. 48, 825–834.
Meyers, S.R., 2007. Production and preservation of organic matter. The significance of iron. Paleoceanography 22, PA4211. http://dx.doi.org/10.1029/2006PA001332.
Meyers, S.R., Siewert, S.E., Singer, B.S., Sageman, B.B., Condon, D.J., Obradovich, J.D., Jicha, B.R., Sawyer, D.A., 2012. Intercalibration of radioisotopic and astrochronologic time scales for the Cenomanian/Turonian boundary interval, Western Interior Basin, USA. Geology 40 (1), 7–10.
Miller, K.G., Kominz, M.A., Browning, J.V., Wright, J.D., Mountain, G.S., Katz, M.E., Sugarman, P.J., Cramer, B.S., Christie-Blick, N., Pekar, S.F., 2005. The Phanerozoic record of global sea-level change. Science 310, 1293–1298 (25 November 2005).
Miller, K.G., Browning, J.V., Boulila, S., Simmons, M.D., 2010. Cold snaps in the greenhouse world: eustasy not tectonics. Geol. Soc. Am. Abstr. Programs 42 (5), 545.
Monger, J.W.H., 1993. Cretaceous tectonics of the North American Cordillera. In: Caldwell, W.G.E., Kauffman, E.G. (Eds.), Evolution of the Western Interior BasinGeol. Assoc. Can. Spec. Pap. 39, 31–47.
National Research Council, 2011. Understanding Earth's Deep Past: Lessons for Our Climate Future. National Academies Press (212 pp.).
Nichols, D.J., Sweet, A.R., 1993. Biostratigraphy of Upper Cretaceous non-marine palynofloras in a north–south transect of the Western Interior Basin. In: Caldwell, W.G.E., Kauffman, E.G. (Eds.), Evolution of the Western Interior BasinGeol. Assoc. Can. Spec. Pap. 39, 539–584.
Nummedal, D., Wolter, N.R., Fleming, T.F., Bergsohn, I., Swift, D.J.P., 1993. Lowstand, shallow marine sandstones in Upper Cretaceous strata of the San Juan Basin, New Mexico. In: Caldwell, W.G.E., Kauffman, E.G. (Eds.), Geol. Assoc. Can. Spec. Pap. 39, 199–218.
Oboh-Ikuenobe, F.E., Benson Jr., D.G., Scott, R.W., Holbrook, J.M., Evetts, M.J., Erbacher, J., 2007. Re-evaluation of the Albian–Cenomanian Boundary in the U.S. Western Interior based on dinoflagellate cysts. Rev. Palaeobot. Palynol. 144, 77–97.
Oboh-Ikuenobe, F.E., Holbrook, J.H., Scott, R.W., Akins, S.L., Evetts, M.J., Benson Jr., D.G., Pratt, L.M., 2008. Anatomy of epicontinental flooding: Late Albian–Early Cenomanian of the Southern U.S. Western Interior. In: Pratt, B.R., Holmden, C. (Eds.), Dynamics of Epeirc SeasGeol. Assoc. Can. Spec. Pap. 48, 201–227.
Obradovich, J.D., 1993. A Cretaceous time scale. In: Caldwell, W.G.E., Kauffman, E.G. (Eds.), Evolution of the Western Interior BasinGeol. Assoc. Can. Spec. Pap. 39, 379–396.
Ogg, J.G., 2012. Geomagnetic polarity time scale. In: Gradstein, F.M., Ogg, J.G., Schmitz, M., Ogg, G. (Eds.), The Geologic Time Scale 2012. Elsevier, pp. 85–113.
Ogg, J.G., Agterberg, F.P., Gradstein, F.M., 2004. The Cretaceous Period. In: Gradstein, F., Ogg, J.G., Smith, A. (Eds.), A Geologic time Scale. Cambridge University Press, Cambridge, U.K., pp. 344–383.
Ogg, J.G., Hinnov, L.A., Huanf, C., 2012. Chapter 7, Cretaceous. In: Gradstein, F.M., Ogg, J.G., Schmitz, M.D., Ogg, G.M. (Eds.), The Geologic Time Scale 2012, vol. 2. Elsevier B.V., Amsterdam, pp. 793–853.
Otofuji, Y.I., 1996. Large tectonic movement of the Japan Arc in late Cenozoic time inferred from paleomagnetism: review and synthesis. Island Arc 5, 229–249.
Otto-Bliesner, B.L., Upchurch, G.R., 1997. Vegetation-induced warming of high-latitude regions during the late Cretaceous period. Nature 385, 804–807.
Otto-Bliesner, B.L., Brady, E.C., Shields, C., 2002. Late Cretaceous ocean: coupled simulations with the National Center for Atmospheric Research climate system model. J. Geophys. Res. - Atmos. 107.
Painter, C.S., 2009. The Shannon Sandstone: New Observations and Constraints Applied to Depositional Models. (M.Sc. Thesis) University of Wyoming (127 pp.).
Parrish, J.T., Gautier, D.L., 1993. Sharon Springs Member of the Pierre Shale: upwelling in the Western Interior Seaway? In: Caldwell, W.G.E. (Ed.), The Cretaceous System in the Western Interior of North AmericaGeol. Assoc. Can. Spec. Pap. 13, 319–332.
Paytan, A., 2004. Seawater sulfur isotope fluctuations in the Cretaceous. Science 304, 1663–1665.
Posamentier, H.W., Vail, P.R., 1988. Eustatic controls on clastic deposition II-Sequence and systems tracts models. In: Wilgus, C.K. (Ed.), Sea-level Changes: An Integrated Approach. Tulsa, Oklahoma: SEPM Special Publication, 42, pp. 125–154.
Pratt, L.M., 1984. Influence of paleoenvironmental factors on preservation of organic matter in Middle Cretaceous Greenhorn Formation, Pueblo, Colorado. AAPG Bull. 68, 1146–1159.
Pratt, L.M., Arthur, M.A., Dean, W.E., Scholle, P.A., 1993. Paleo-oceanographic cycles and events during the Late Cretaceous in the Western Interior Seaway of North America. In: Caldwell, W.G.E., Kauffman, E.G. (Eds.), Evolution of the Western Interior BasinGeol. Assoc. Can. Spec. Pap. 39, 333–354.
Pucéat, E., Lécuyer, C., Sheppard, S.M.F., Dromart, G., Rebolet, S., Grandjean, P., 2003. Thermal evolution of Cretaceous Tethyan marine waters inferred from oxygen isotope composition of fish tooth enamels. Paleoceanography 18, 1029–1041. http://dx.doi.org/10.1029/2002PA000823.
Pucéat, E., Lécuyer, C., Reisberg, L., 2005. Neodymium isotope evolution of NW Tethyan upper ocean waters throughout the Cretaceous. Earth Planet. Sci. Lett. 236, 705–720.
Ren, J.Y., Tamaki, K., Li, S.T., Zhang, J.X., 2002. Late Mesozoic and Cenozoic rifting and its dynamic setting in Eastern China and adjacent areas. Tectonophysics 344 (3-4), 175–205.
Ronov, A.B., 1994. Phanerozoic transgressions and regressions on the continents: a quantitative approach based on areas flooded by the sea and areas of marine and continental deposition. Am. J. Sci. 294, 777–801.

Ronov, A.B., Khain, V.E., Balukhovsky, A.N., 1989. In: Barsukhov, V.L., Laviorov, N.P. (Eds.), Atlas of Lithological–Paleogeographical Maps of the World: Mesozoic and Cenozoic of Continents and Oceans. Editorial Publishing Group, Moscow, pp. 1–79.
Royse Jr., F., Warner, M.A., Reese, D.L., 1975. Thrust belt structural geology and related stratigraphic problems, Wyoming–Idaho–northern Utah. In: Bolyard, D.W. (Ed.), Deep Drilling Frontiers of the Central Rocky Mountains. Rocky Mountain Association of Geologists, pp. 41–54.
Sageman, B.B., 1985. High-resolution stratigraphy and paleobiology of the Hartland Shale Member: analysis of an oxygen-deficient epicontinental sea. In: Pratt, L.M., Kauffman, E.G., Zelt, F.B. (Eds.), Fine-grained Deposits and Biofacies of the Cretaceous Western Interior Seaway: Evidence of Cyclic Sedimentary Processes. Society of Economic Paleontologists and Mineralogists, Field Trip Guidebook No. 4, 1985 Midyear Meeting, Golden, Colorado, pp. 110–121.
Sageman, B.B., Rich, J., Arthur, M.A., Birchfield, G.E., Dean, W.E., 1997. Evidence for Milankovitch periodicities in Cenomanian–Turonian lithologic and geochemical cycles, Western Interior U.S.A. J. Sediment. Res. 67, 286–301.
Sageman, B.B., Rich, J., Arthur, M.A., Dean, W.E., Savrda, C.E., Bralower, T.J., 1998. Multiple Milankovitch cycles in the Bridge Creek Limestone (Cenomanian–Turonian), Western Interior Basin. In: Dean, W.E., Arthur, M.A. (Eds.), Stratigraphy and Paleoenvironments of the Cretaceous Western Interior Seaway. SEPM (Society for Sedimentary Geology) Concepts in Sedimentology and Paleontology, 6, pp. 153–171.
Sageman, B.B., Meyers, S.R., Arthur, M.A., 2006. Orbital time scale and new C-isotope record for Cenomanian–Turonian boundary stratotype. Geology 34, 125–128. http://dx.doi.org/10.1130/G22074.1.
Scherer, J., Upchurch, G.R., Knaus, M.J., Mack, G.H., 2002. How Consistently Do Regression Models of Foliar Physiognomy Predict Cretaceous Climates? Workshop on Cretaceous Climate and Ocean Dynamics, Florissant, Colorado, USA.
Schlanger, S.O., Jenkyns, H.C., 1976. Cretaceous oceanic anoxic events—causes and consequences. Geol. Mijnb. 55, 179–184.
Schlanger, S.O., Arthur, M.A., Jenkyns, H.C., Scholle, P.A., 1987. The Cenomanian–Turonian oceanic anoxic event, I. Stratigraphy and distribution of organic carbon-rich beds and the marine ^{13}C excursion. In: Brooks, J., Fleet, A. (Eds.), Marine Petroleum Source RocksGeol. Soc. Lond., Spec. Publ. 26, 371–399.
Schröder-Adams, C.J., Herrle, J.O., Tu, Q., 2012. Albian to Satonian carbon isotope excursions and faunal extinctions in the Canadian Western Interior Sea: recognition of eustatic sea-level controls on a forebulge setting. Sed. Geol. 281, 50–58.
Schwans, P., 1995. Controls on sequence stacking and fluvial to shallow-marine architecture in a foreland basin. AAPG Mem. 64, 54–102.
Scotese, C.R., 2002. http://www.scotese.com (PALEOMAP website).
Scott, R.W., 2009. Chronostratigraphic database for Upper Cretaceous oceanic red beds (CORBs). In: Wang, C., Hu, X., Scott, R.W., Wagriech, M., Jansa, L. (Eds.), Cretaceous Oceanic Red Beds: Stratigraphy, Composition, Origins, and Paleoceanographic and Paleoclimatic SignificanceSEPM Spec. Publ. 91, 35–57.
Scott, R.W., Franks, P.C., Evetts, M.J., Bergen, J.A., Stein, J.A., 1998. Timing of Mid-Cretaceous relative sea level changes in the Western Interior: Amoco No. 1 Bounds Core. In: Dean, W.E., Arthur, M.A. (Eds.), Stratigraphy and Paleoenvironments of the Cretaceous Western Interior Seaway, USA. SEPM Concepts in Sedimentology and Paleontology, 6, pp. 11–34.
Scott, R.W., Holbrook, J.M., Oboh-Ikuenobe, F.E., Evetts, M.J., Benson, D.G., Kues, B.S., 2004. Middle Cretaceous stratigraphy, southern Western Interior seaway, New Mexico and Oklahoma. Mt. Geol. 41, 33–61.
Scott, R.W., Wan, X., Wang, C., Huang, Q., 2012. Late Cretaceous chronostratigraphy (Turonian–Maastrichtian): SK1 Core Songliao Basin, China. Geosci. Front. http://dx.doi.org/10.1016/j.gsf.2012.02.004.
Şengör, A.M.C., Natal'in, B.A., 1996. Palaeotectonics of Asia: fragments of a synthesis. In: Yin, A., Harrison, T.M. (Eds.), The Tectonic Evolution of Asia. Cambridge Univ. Press, Cambridge, pp. 486–640.
Sewall, J.O., van der Wal, R.S.W., van der Zwan, K., van Oosterhout, C., Dijkstra, H.A., Scotese, C.R., 2007. Climate model boundary conditions for four Cretaceous time slices. Clim. Past 3, 647–657.
Sha, J.G., 2007. Cretaceous stratigraphy of northeast China: non-marine and marine correlation. Cretac. Res. 28, 146–170.
Sha, J.G., Hirano, H., Yao, X.G., Pan, Y.H., 2008. Late Mesozoic transgressions of eastern Heilongjiang and their significance in tectonics, and coal and oil accumulation in northeast China. Palaeogeogr. Palaeoclimatol. Palaeoecol. 263, 119–130.
Skelton, P.W., Spicer, R.A., Kelley, S.P., Gilmour, I., 2003. The Cretaceous World. Cambridge University Press, Cambridge, UK.
Sladen, C.P., 1994. Key elements during the search for hydrocarbons in lake systems. In: Gierlowski-Kordesch, E., Kelts, K. (Eds.), Global Geological Record of Lake Basins, 1. Cambridge University Press, pp. 3–17.
Slingerland, R., Kump, L.R., Arthur, M.A., Fawcett, P.J., Sageman, B.B., Barron, E.J., 1996. Estuarine circulation in the Turonian Western Interior seaway of North America. GSA Bull. 108 (7), 941–952.
Sloss, L.L., 1963. Sequences in the cratonic interior of North America. Geol. Soc. Am. Bull. 74, 93–114.
Smit, J., van der Kaars, S., 1984. Terminal Cretaceous extinctions in the Hell Creek Area, Montana: compatible with catastrophic extinction. Science 223, 1177–1179.
Spicer, R.A., Herman, A.B., 2010. The Late Cretaceous environment of the Arctic: a quantitative reassessment based on plant fossils. Palaeogeogr. Palaeoclimatol. Palaeoecol. 295, 423–442.
Stoll, H.M., Schrag, D.P., 2000. High-resolution stable isotope records from the Upper Cretaceous rocks of Italy and Spain: glacial episodes in a greenhouse planet? Geol. Soc. Am. Bull. 112, 308–319.
Trabucho Alexandre, J., Tuenter, E., Henstra, G.A., van der Zwan, K.J., van de Wal, R.S.W., Dijkstra, H.A., de Boer, P.L., 2010. The mid-Cretaceous North Atlantic nutrient trap: Black shales and OAEs. Paleoceanography 25, PA4201. http://dx.doi.org/10.1029/2010PA001925.
Tyrrell, T., 1999. The relative influences of nitrogen and phosphorus on oceanic primary production. Nature 400, 525–531.
Upchurch Jr., G.R., Wolfe, J.A., 1993. Cretaceous vegetation of the Western Interior and adjacent regions of North America. In: Caldwell, W.G.E. (Ed.), The Cretaceous System in the Western Interior of North AmericaGeol. Assoc. Can. Spec. Pap. 13, 243–281.
Upchurch, G.R., Otto-Bliesner, B.L., Scotese, C.R., 1998. Vegetation-atmosphere interactions and their role in global warming during the latest Cretaceous. Philos. Trans. R. Soc. Lond. B 353, 97–112.
Van Cappellen, P., Ingall, E.D., 1994. Benthic phosphorus regeneration, net primary production and ocean anoxia: a model of coupled marine biogeochemical cycles of carbon and phosphorus. Paleoceanography 9, 677–692.
Van Wagoner, J.C., Mitchum, R.M., Campion, K.M., Rahmanian, V.D., 1990. Siliciclastic sequence stratigraphy in well logs, cores, and outcrops: concepts for high-resolution correlation of time and facies. American Association of Petroleum Geologists Methods in Exploration, 7 (55 pp.).
Wagner, T., Hofmann, P., Flögel, S., 2013. Marine black shale deposition and Hadley Cell dynamics: a conceptual framework for the Cretaceous Atlantic Ocean. Mar. Pet. Geol. 43, 222–238.
Wagreich, M., Bojar, Ana-Voica, Sachsenhofer, R.F., Neuhuber, S., Egger, H., 2008. Calcareous nannoplankton, planktonic foraminiferal, and carbonate carbon isotope stratigraphy of the Cenomanian–Turonian boundary section in the Ultrahelvetic Zone (Eastern Alps, Upper Austria). Cretac. Res. 29, 965–975.
Walaszczyk, I., Cobban, W.A., 2000. Inoceramid faunas and biostratigraphy of the Upper Turonian–Lower Coniacian of the Western Interior of the United States. Palaeontolofical Association Special Papers in Palaeontology, 64 1–118.
Walaszczyk, I., Cobban, W.A., 2007. Inoceramid fauna and biostratigraphy of the upper Middle Coniacian–Lower Middle Santonian of the Pueblo section, (SE Colorado, US Western Interior). Cretac. Res. 28, 132–142.
Wan, X.Q., Zhao, J., Scott, R.W., Wang, P.J., Feng, Z.H., Huang, Q.H., Xi, D.P., 2013. Late Cretaceous Stratigraphy, Songliao Basin, NE China: SK1 cores. Palaeogeogr. Palaeoclimatol. Palaeoecol. 385, 31–43.
Wang, P.J., Liu, W.Z., 2001. Depositional Events: Introduction, Example and Application. Jilin Scientific and Technical Press, Changchun 1–182.
Wang, P.J., Du, X.D., Wang, D.P., 1995. Geochemical records of the Cretaceous lacustrine transgressive sequences and the marine-lake connecting events in the Songliao Basin, Northeast China. Sediment. Facies Paleogeogr. 15 (4), 14–20 (in Chinese with English abstract).
Wang, X., Feng, Z.H., Fang, W., Huo, Q.L., 2006. The Cretaceous Paleoclimate Change and the Formation of Mass Source Rock in the Songliao Basin. Unpublished report Daqing Oilfield Company.
Wang, C.S., Feng, Z.Q., Wu, H.Y., Wang, P.J., Kong, F.J., Feng, Z.H., Ren, Y.G., Yang, G.S., Wan, X.Q., Huang, Y.J., Zhang, S.H., 2008. Preliminary achievement of the Chinese Cretaceous continental scientific drilling Project-SK-I. Acta Geol. Sin. 82 (1), 9–20 (in Chinese with English abstract).
Wang, G.D., Cheng, R.H., Wang, P.J., Gao, Y.F., Wang, C.S., Ren, Y.G., Huang, Q.H., 2009a. Description of Cretaceous sedimentary sequence of the Quantou Formation recovered by CCSD-SK-Is borehole in Songliao Basin: lithostratigraphy, sedimentary facies and cyclic stratigraphy. Earth Sci. Front. 16 (2), 324–338.
Wang, P.J., Gao, Y.F., Cheng, R.H., Wang, G.D., Wu, H.Y., Wan, X.Q., Yang, G.S., Wang, Z.X., 2009b. Description of Cretaceous sedimentary sequence of the second and third member of the Qingshankou Formation recovered by CCSD-SK-Is borehole in Songliao Basin: lithostratigraphy, sedimentary facies and cyclic stratigraphy. Earth Sci. Front. 16 (2), 288–313.
Wang, C.S., Feng, Z.Q., Zhang, L.M., Huang, Y.J., Cao, K., Wang, P.J., Zhao, B., 2013. Cretaceous paleogeography and paleoclimate and the setting of SKI borehole sites in Songliao Basin, northeast China. Palaeogeogr. Palaeoclimatol. Palaeoecol. 385, 17–30.
Warren, J., 2000. Dolomite: occurrence, evolution and economically important associations. Earth Sci. Rev. 52, 1–81.
White, T., Arthur, M.A., 2006. Organic carbon production and preservation in response to sea-level changes in the Turonian Carlile Formation, U.S. Western Interior Basin. Palaeogeogr. Palaeoclimatol. Palaeoecol. 235, 223–244.
Whittaker, S.G., Kyser, T.K., Caldwell, W.G.E., 1987. Paleoenvironmental geochemistry of the Claggett marine cyclothem in south–central Saskatchewan. Can. J. Earth Sci. 24, 967–984.
Wilkin, R.T., Barnes, H.L., 1996. Pyrite formation by reactions of iron monosulfides with dissolved inorganic and organic sulfur species. Geochim. Cosmochim. Acta 60, 4167–4179.
Wolfe, J.A., Upchurch, J.R., G.R., 1987. North American marine climates and vegetation during the Late Cretaceous. Palaeogeogr. Palaeoclimatol. Palaeoecol. 61, 33–77.
Wu, H.C., Zhang, S.H., Jiang, G.Q., Huang, Q.H., 2009. The floating astronomical time scale for the terrestrial Late Cretaceous Qingshankou Formation from the Songliao Basin of Northeast China and its stratigraphic and paleoclimate implications. Earth Planet. Sci. Lett. 278, 308–323.
Wu, H.C., Zhang, S.H., Jiang, G.Q., Hinnov, L., Yang, T.S., Li, H.Y., Wan, X.Q., Wang, C.S., 2013. Astrochronology of the Early Turonian–Early Campanian terrestrial succession in the Songliao Basin, northeastern China and its implication for long-period behavior of the Solar System. Palaeogeogr. Palaeoclimatol. Palaeoecol. 385, 55–70.
Xi, D.P., Wan, X.Q., Feng, Z.Q., Li, S., Feng, Z.H., Jia, J.Z., Jin, X., Si, W.M., 2011a. Discovery of Late Cretaceous foraminifera in the Songliao Basin: evidence from SK-1 and implications for identifying seawater incursions. Chin. Sci. Bull. 55 (35), 3433–3436 (in Chinese with English abstract).
Xi, D.P., Li, S., Wan, X., Jing, X., Huang, Q., Colin, J.P., Wang, Z., Si, W., 2011b. Late Cretaceous biostratigraphy and paleoenvironmental reconstruction based on non-marine

ostracodes from well SK1 (south), Songliao Basin, northeast China. Hydrobiologia. http://dx.doi.org/10.1007/s10750-011-0765-6 (11 pp.).
Xiang, F., Song, J.C., Luo, L., Tian, X., 2009. Distribution characteristics and climate significance of continental special deposits in the Early Cretaceous. Earth Sci. Front. 16, 48–62 (in Chinese with English abstract).
Yang, W.L., Gao, R.Q., Guo, Q.F., Liu, S.G., 1985. Generation, Migration and Accumulation of Terrestrial Oil in the Songliao Basin. Heilongjiang Scientific and Technological Press, Harbin 50–158 (in Chinese with English Abstract).
Ye, D.Q., Huang, Q.H., Zhang, Y., Chen, C.R., 2002. Cretaceous Ostracoda Biostratigraphy in Songliao Basin. Petroleum Industry Press, Beijing 11–144 (in Chinese with English abstract).
Yin, A., Nie, S., 1996. A Phanerozoic palinspastic reconstruction of China and its neighboring regions. In: Yin, A., Harrison, T.M. (Eds.), The Tectonic Evolution of Asia. Cambridge Univ. Press, Cambridge, pp. 442–485.
Zakharov, Y.D., Boriskina, N.G., Ignatyev, A.V., Tanabe, K., Shigeta, Y., Popov, A.M., Afanasyeva, T.B., Maeda, H., 1999. Palaeotemperature curve for the Late Cretaceous of the northwestern circum-Pacific. Cretac. Res. 20, 685–697.
Zakharov, Y.D., Popov, A.M., Shigeta, Y., Smyshlyaeva, O.P., Sokolova, E.A., Nagendra, R., Velivetskaya, T.A., Afanasyeva, T.B., 2006. New Maastrichtian oxygen and carbon isotope record: additional evidence for warm low latitudes. Geosci. J. 10, 347–367.
Zhang, M.M., Zhou, J.J., Liu, Z.C., 1977. Age and deposition environment of Cretaceous fish fossil-bearing strata in NE China. Vertebr. Anthropol. 15, 194–197 (in Chinese with English Abstracts).
Zhang, X.Z., Yang, B.J., Wu, F.Y., Liu, G.X., 2006. The lithosphere structure in the Hingmong–Jihei (Hinggan–Mongolia–Jilin–Heilongjiang) region, northeastern China. Geol. China 33 (4), 816–823.
Zheng, J.Y., Yin, Y.H., Li, B.Y., 2010. A new scheme for climate regionalization in China. Acta Geograph. Sin. 65, 3–12 (in Chinese with English Abstracts).
Zhu, R.X., Shao, J.A., Pan, Y.X., Shi, R.P., Shi, G.H., Li, D.M., 2002. Paleomagnetic data from the Early Cretaceous volcanic rocks of west Liaoning: evidence for intra-continental rotation. Chin. Sci. Bull. 47, 1335–1440 (in Chinese).
Zorin, Y.A., 1999. Geodynamics of the western part of the Mongolia–Okhotsk collisional belt, Trans-Baikal region (Russia) and Mongolia. Tectonophysics 306, 33–56.